



# CHALMERS

## **2D hybrid modeling of defects in an ultrasonic inspection situation**

MARIA SEMENOVA



THESIS FOR THE DEGREE OF LICENTIATE OF ENGINEERING IN SOLID  
AND STRUCTURAL MECHANICS

2D hybrid modeling of defects in an ultrasonic inspection  
situation

MARIA SEMENOVA

Department of Industrial and Materials Science (IMS)  
Division of Engineering Materials  
CHALMERS UNIVERSITY OF TECHNOLOGY  
Göteborg, Sweden 2021

2D hybrid modeling of defects in an ultrasonic inspection situation  
MARIA SEMENOVA

© MARIA SEMENOVA, 2021

ISSN 1652-8565

Department of Industrial and Materials Science (IMS)

Division of Engineering Materials

Chalmers University of Technology

SE-412 96 Göteborg

Sweden

Telephone: +46 (0)31-772 1000

Chalmers Reproservice  
Göteborg, Sweden 2021

2D hybrid modeling of defects in an ultrasonic inspection situation

MARIA SEMENOVA

Department of Industrial and Materials Science (IMS)

Division of Engineering Materials

Chalmers University of Technology

## ABSTRACT

Advanced methods of nondestructive evaluations (NDE) are widely used for in-service inspection in many industrial applications, e.g. nuclear and aerospace industries. In these applications the components are exposed to different degradation mechanisms (e. g. fatigue, corrosion, stress corrosion cracking). In-service caused defects such as fatigue and stress corrosion cracks can be sized and monitored in order to postpone repairs or replacements.

The reliability of NDE methods and the interaction between applied energy and addressed defect is highly dependent on the equipment adjustment to a specific object and to the expectation of the crack features. The crack feature and morphology vary widely between different crack mechanisms and between material types, in which crack appears.

Complex shaped defects, such as fatigue and stress corrosion cracks (SCC), are in many cases difficult to characterize with ultrasonic NDE methods. SCC has in many cases a heavily branched macroscopic shape with a large number of crack tips. Ultrasonic NDE method is not always reliable in sizing such defects, as the diffraction from the crack tips is commonly used as the basis for such analysis. In this case, thoroughly validated mathematical models could be used to do the parametrical studies that address such interactions.

In the current work, a developed hybrid model is described. This model is based on a combination of a semi-analytical model with a numerical approach. The basic idea is to use the numerical solution for interaction between the wave and the complex shape defect, which could be done by surrounding it with a volume modelled by a finite element scheme. The analytical method is used for describing the wave propagation between the probe and the volume that contains the actual defect.

Using hybrid models for parametrical study, could help to avoid costly and time-consuming experimental work.

Keywords: T matrix, Finite element method, Modelling, Scattering, Ultrasonics



## PREFACE

This thesis includes the work conducted during the year 2017 - 2021, which is part of a research project *Mathematical modeling of fatigue and stress corrosion crack*. This research project is sponsored by the Swedish Radiation Safety Authority, SSM. The actual work was carried out at the research group of Advanced Nondestructive Testing, department of Industrial and Materials Science, Chalmers.

Studying and doing research at Chalmers is a great experience for me. First, I would like to give a warm thanks to my supervisor Professor Håkan Wirdelius for his great help and support along the way. Next, I wish to express my gratitude to Gert Persson, who used to be my assistant supervisor, and who helped me a lot by sharing his expertise in finite element modelling and for contributing to fruitful discussions. Also, I would like to thank our research group of Advanced Nondestructive Testing for very joyful working environment.

Finally, I owe gratitude to my parents, who always support and encourage me.

Gothenburg, 2021

Maria Semenova





# THESIS

This thesis consists of an extended summary and the following appended papers:

**Paper A**      Maria Semenova, Håkan Wirdelius, Gert Persson. "Comparison between three mathematical models of three well defined ultrasonic NDT cases". *Published in conference proceedings*

**Paper B**      Maria Semenova, Håkan Wirdelius. "Parametrical study in hybrid modeling of an ultrasonic inspection situation". *To be submitted*

The appended papers were collaboratively prepared with co-authors. The author of this thesis was responsible for the major progress of the work, i.e. creating models in different software, doing simulations, post-processing and writing of the papers, all with the assistance of the co-authors.



# CONTENTS

<b>Abstract</b>	<b>i</b>
<b>Preface</b>	<b>iii</b>
<b>Thesis</b>	<b>v</b>
<b>Contents</b>	<b>vii</b>
<b>I Extended Summary</b>	<b>1</b>
<b>1 Introduction</b>	<b>1</b>
1.1 Background . . . . .	1
1.2 Aims and limitations . . . . .	4
1.3 Thesis structure . . . . .	4
<b>2 Technical Background</b>	<b>5</b>
2.1 Ultrasonic Testing (UT) . . . . .	5
2.1.1 Basic principles of ultrasonic testing . . . . .	5
2.1.2 Wave types . . . . .	7
2.1.3 Probe model . . . . .	8
2.1.4 Statement of the problem . . . . .	9
2.2 Analytical solution . . . . .	10
2.2.1 Elastic waves . . . . .	10
2.2.2 T matrix . . . . .	12
2.2.3 Expansion coefficients for incoming wave . . . . .	13
2.2.4 Expansion coefficients for scattered wave . . . . .	14
<b>3 Numerical solution</b>	<b>16</b>
3.1 Considered software . . . . .	16
3.1.1 simSUNDT . . . . .	16
3.1.2 k-Wave toolbox . . . . .	17
3.1.3 COMSOL Multiphysics . . . . .	18
3.2 Validation and comparison of the results . . . . .	19
3.2.1 Paper A . . . . .	19

<b>4</b>	<b>Hybrid modelling</b>	<b>21</b>
4.1	Determination of T matrix . . . . .	22
4.2	Validation and comparison results . . . . .	24
4.2.1	Paper B . . . . .	24
<b>5</b>	<b>Summary of appended papers</b>	<b>29</b>
5.1	Paper A . . . . .	29
5.2	Paper B . . . . .	29
<b>6</b>	<b>Conclusion and future plans</b>	<b>31</b>
	<b>References</b>	<b>32</b>
<b>II</b>	<b>Appended Papers A–B</b>	<b>35</b>

# Part I

## Extended Summary

### 1 Introduction

Nowadays, advanced methods of nondestructive evaluation (NDE) and nondestructive testing (NDT) are commonly used for in-service inspection in many areas, such as nuclear and aerospace industries. NDE could be used to determine and locate flaws and leaks, to estimate chemical composition, mechanical and physical properties of the material and to verify and control processing ( e. g. heat treating). Individual components might be exposed to different degradation mechanisms (e. g. fatigue, corrosion, stress corrosion cracking), and NDE could be used to evaluate the integrity of individual components. In-service induced defects such as fatigue and stress corrosion cracks can, if they are detected, be sized and monitored in order to postpone repairs or replacements. Such defects become more and more essential to address as the power plants are exploited beyond their estimated lifetimes in combination with an increase of power outage in recent years.

#### 1.1 Background

Defects, such as fatigue or stress corrosion cracks, appeared in the machinery parts during operation need to be detected, sized and monitored, in order to postpone the repairs or replacement. Nondestructive testing (NDT) methods are commonly used in the industry for that purpose. It is important to clarify that the term NDT is generally refers to the actual testing only. Nondestructive evaluation (NDE) is used, when the procedure and calibration are described. The full testing procedure, which includes testing method, calibration process and the interpretation of the obtained results, such as characterization, sizing and positioning of the defect, is considered in Quantitative Nondestructive Evaluation (QNDE) [1]. Even though these terms have different definitions, most of the time NDT, NDE and QNDE are interchangeable and implies to the broadest one. In this work term NDT is considered to be the broadest.

For selecting an NDT method several criteria need to be considered:

1. What is going to be inspected: material properties, a discontinuity (a void or a crack), sheet or coating thickness;
2. Which physical process are used in the NDT method;

3. How the interaction between the probing field with the test material takes place;
4. Which advantages and limitations chosen NDT method has;
5. Other important factors, such as economic, environmental or others.

To make the correct choice of the suitable NDT method for each specific case it is important to be aware of the potentials and limitations of the existing technology. All NDT methods could be divided in two groups, based on the areas of application: surface and in-depth penetration. Magnetic particle and penetrant testing belong to the first group, and could only be used for the surface inspection, when it is necessary to check component for the surface cracks, which are not possible to identify with naked eye. The main features of these methods are rapid, simple and inexpensive testing, portable and possible to used in remote locations, some requirements for materials and only suitable for identifying surface cracks. The second group includes radiographic and ultrasound testing, which could be used for scanning internal defects in the components. Both methods have less limitations of the material requirements and could be used for measuring density and material properties. Radiographic testing is visual and could be used for rapid area inspections, but at the same time this method can be hazardous, expensive and requires highly skilled operator. The main features of ultrasound inspection: high penetration depth, sensitivity, accuracy. This inspection is safe, and due to the small size of the equipment, it is quite portable. Although, the interpretation of the results requires significant operator training, and there are limitations in the shape and size of defects, which could be found with this procedure. Eddy current testing could be considered as a part of both groups, because it is used for detecting surface and near surface defects. Inspection gives immediate results, sensor is very sensitive to small cracks, equipment is very portable, but it only can be used for conductive materials.

The reliability of NDT methods is highly dependent on the equipment adjustment to a specific object and to the expectation of the crack features. The crack feature and morphology vary widely between different crack mechanisms and between material types, in which crack appears. Since all these NDT methods are indirect and based on prior information on signal into the component, some kind of interpretation of received signal is always the basis for judgment of the quality of the component. The different degradation mechanisms produce very different kind of cracks or defects in a 3D morphological perspective. Therefore, they interact and influence the received signal in an individual manner.

Stress corrosion cracks (SCC) and fatigue cracks are the most common and critical defects that appeared in the nuclear industry. SCC tends to have a heavily branched macroscopic shape with a large number of crack tips. The diffraction

from the cracks tips is used as the basis for the defect size analysis, and ultrasonic NDT methods are not always reliable in in this kind of application. In this case, mathematical modelling could be used to do the parametrical studies that address such interactions and dependencies that never would be possible to achieve by experiments.

Instead of costly and complicated experiments, a thoroughly validated mathematical models can be used. Such models are very useful in development of parametric studies and in the qualification of testing procedures. However, up to this date only a couple of models have been developed that cover the whole testing procedure, e.g. they include the modeling of transmitting and receiving probes, the scattering by defects and the calibration. Chapman [2] employs geometrical theory of diffraction for some simple crack shapes and Fellingner et al [3] have developed a type of finite integration technique for a two-dimensional treatment of various types of defects. Lhémy et al [4] employs Kirchhoff's diffraction theory that enables their model to handle more complex geometries in 3D. In the literature, Gray et al [5] and Achenbach [6] presents overviews of ultrasonic NDT models. Boström and Wirdelius [7] presented a model based on the T matrix concept, in principle without any approximation, see e. g. Bøvik and Boström [8] for similar work for cracks. However, it is limited to address only simple shaped defects. In Westlund and Boström [9] a 2D hybrid model of a defect near the back surface is deduced.

A two-dimensional hybrid method, combining finite element method (FEM) and an integral representation, is used in this study to predict ultrasonic interaction with a defect. Mathematical modelling of NDT techniques is also essential when it comes to quantifying the capacity of a specific procedure and technique (NDE) in a specific application.

A fundamental problem with modelling in-service induced cracks is that each defect is individual with a unique morphology created by a unique stress and chemical environmental progress. Since these specific features of such cracks cannot be prescribed without a large amount of uncertainty, the conventional way to model these cracks is to generalize into a very simplified and idealized geometric shape.

The hybrid method takes advantage of both semi-analytical and numerical approaches. The basic idea is to surround the defect by a finite element scheme and deal with the propagation between the probe and the defect with a semi analytical method. In this way it is possible to model more complex crack geometries that involves a complicated scattering processes without getting to large numerical models. Where it is possible to implement, semi-analytical and fully numerical approaches are complementary.

## 1.2 Aims and limitations

This thesis is part of a research project *Mathematical modeling of fatigue and stress corrosion crack*, the main purpose of which is to develop a two-dimensional hybrid model. It will allow to do a simulation of ultrasonic scattering from a crack like structure and develop a three dimensional model, which will be able to simulate a situation with a more complicated geometry of the modeled defect (SCC). To accomplish this goal, the mathematical models of ultrasonic wave propagation and the software based on finite element method (FEM) should be studied. Comparison between three software is presented in appended Paper A. The discrete modeling, made by using two different approaches, FE-modeling by using of COMSOL Multiphysics<sup>®</sup> and a finite difference method by applying k-Wave toolbox for MATLAB<sup>®</sup> were considered in the paper.

As the next step of the project, it is important to create and validate a two-dimensional hybrid model for simple shaped defect (e. g. cavity), which the present work is focused on. The most complicated parts are to get a good correlation between the analytical solution and the chosen FEM software and to combine equations with the values received from the software. In Paper B the developing of the hybrid model is described. The model is based on the combining numerical and analytical approaches. For the numerical simulations COMSOL Multiphysics<sup>®</sup> was used. The analytical solution and the hybrid model were done in the MATLAB<sup>®</sup>.

Some obvious limitations do exist, when the analytical equations are combined with values received from numerical solution. Some of the approximations used in FEM solution might have too big influence on the hybrid model solution and might provide error source to the final results.

## 1.3 Thesis structure

This thesis is structured in following sections according to the aims. Section 1 provides background information as well as the objectives and limitations of the current work. Section 2 introduces basic knowledge related to the ultrasonic testing method and the analytical model. Next Section 3 introduces the hybrid method, gives an overview of the used software and a summary of Paper A. Section 4 describes the developed hybrid model and introduces the results from Paper B. Section 5 lists the summary of the appended papers, and Section 6 contains some concluding remarks and the future direction of work.



## 2 Technical Background

### 2.1 Ultrasonic Testing (UT)

#### 2.1.1 Basic principles of ultrasonic testing

The ultrasonic testing (UT) method is based on the ability of ultrasonic waves to propagate in solids, and as the waves travel, they interact with solids in ways that we can predict and represent mathematically. UT inspection can thus be used to describe nature of a solid material (thickness, flaws, elasticity, etc) [1].

The conventional UT probe consists of the piezoelectric element which converts electrical signals into mechanical vibrations (transmit mode) and mechanical vibrations into electrical signals (receive mode). In general, piezoelectric transducers are set up to vibrate at the fundamental frequency. Piezoelectric transducers need some sort of coupling medium to transmit the ultrasound between the transducer and the test specimen, due to the large acoustic impedance mismatch between the transducer and air. Grease, gels, liquids, special high-viscosity material could be used as a coupling to help certain wave type to propagate into the medium.

Real material is inhomogeneous and can contain structure irregularities, such as: porosity, inclusions, phase changes in metals or ceramics, grain structure, and the change from one constituent material to another in composite materials. When a wave collides with these material variations, it can reflect, refract, or transform modes according to the angle of incidence, change in density, and change in elastic properties. Thus, it is obvious, that there is a special inspection procedure to identify different defects, and in each case the shape of the scattered wave is also different. For example, wave scattered from the surface of the cavity differs a lot from one scattered from the crack tip.

The stress corrosion cracks (SCC) often tends to have a heavily branched macroscopic shape with a large number of crack tips, see Figure 2.1. As the diffraction from the crack tips is commonly used as the basis for the defect size analysis ultrasonic NDT methods are not always reliable in this kind of applications. The scattered wave signal becomes too noisy, so it is impossible to analyze it [10].

The scattered waves can travel in all directions depending on the property of the hit object and some of them returns to the probe. After the piezoelectric element receives the scattered waves, it converts them back to an electrical pulse, which is then amplified as the output signal. This signal is represented as pulse amplitude versus elapsed time. Ultrasonic inspection directly measures four variables: time of flight, amplitude, phase and frequency. All other information is derived from this set of variables. Therefore, the ultrasonic testing method, as all other NDT methods, is indirect, since the measured output data comes in the

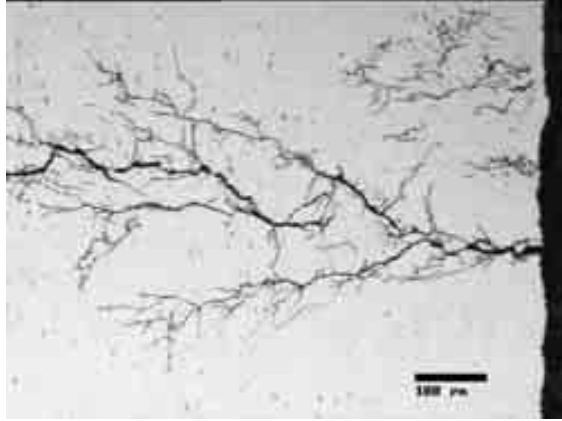


Figure 2.1: *Typically branched shape of TGSCC in austenitic stainless steels [11]*

form of quantitative information, which requires further interpretations.

There are several existing UT methods, which are used for specific cases [1]:

- Pulse-echo ultrasonic measurements can be used to determine the location of a discontinuity in a part or structure by accurately measuring the time required for a short ultrasonic pulse generated by a transducer to travel through a thickness of material, reflect from the back or the surface of a discontinuity, and be returned to the transducer.
- Angle Beam Transducers and wedges are typically used to introduce a refracted shear wave into the test material. An angled sound path allows the sound beam to come in from the side, thereby improving detectability of flaws in and around welded areas.
- Ultrasonic scanning systems are used for automated data acquisition and imaging. The signal strength and the time-of-flight of the signal is measured for every point in the scan plan. The most common ultrasonic scanning systems involve the use of an immersion tank. The ultrasonic transducer and the part are placed under water so that consistent coupling is maintained by the water path as the transducer or part is moved within the tank.
- Laser ultrasonic systems use laser beams to generate the ultrasound and collect the resulting signals in a noncontact mode. Advances in transducer technology has lead to the development of an inspection technique known as air-coupled ultrasonic inspection. These systems are capable of sending ultrasonic energy

through air and getting enough energy into the part to have a useable signal. These system typically use a through-transmission technique since reflected energy from discontinuities are too weak to detect.

### 2.1.2 Wave types

The elastodynamic waves propagating in the solid medium can be divided into four types of waves: *longitudinal* waves, *transverse* waves, surface waves and plate waves in thin materials.

The main difference between the first two is the direction of movement of the medium particles, see Figure 2.2. *Longitudinal* (P-wave), which also called pressure wave, cause the parallel motion to the direction of propagation. The displacement of the *transverse* waves (S-waves) are usually located in the perpendicular direction of wave propagation and are designated as horizontally (SH) and vertically (SV) polarized waves [12].

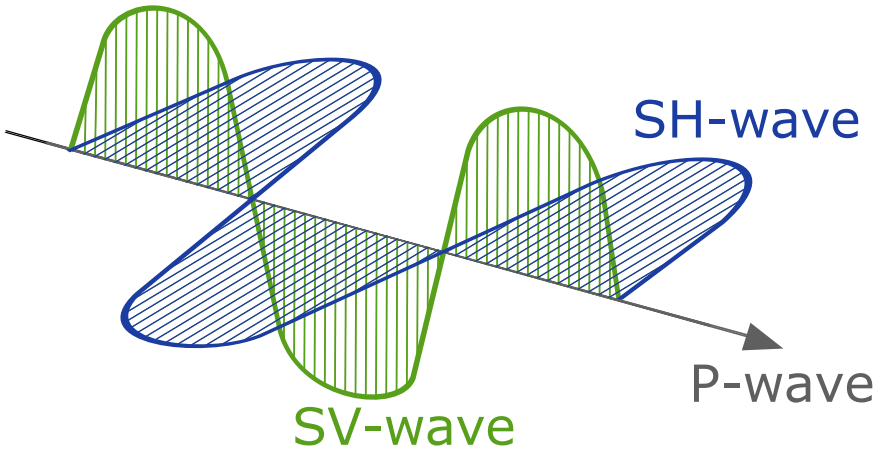


Figure 2.2: *Propagating wave in the solid medium*

Surface (or *Rayleigh*) waves could appear in the a relatively thick solid material, and are penetrating to a depth of one wavelength. Surface waves combine both a longitudinal and transverse motion to create an elliptic orbit motion. Rayleigh waves are very sensitive to surface defects and can follow the surface around curves.

Plate waves (*Lamb* waves) are similar to surface waves except they can only be generated in materials a few wavelengths thick. *Lamb* waves are complex vibrational waves that propagate parallel to the test surface throughout the thickness of the material. Propagation of *Lamb* waves depends on the density and the elastic material properties of a component and also influenced by the test

frequency and material thickness. The complex motion of the particles is similar to the elliptical orbits for surface waves (symmetrical and asymmetrical mode).

All these waves could be used for conventional UT inspection purposes. The influence of surface and plate waves could be ignored if the testing component is thick and the defects are located far from the surface.

### 2.1.3 Probe model

As was described in 2.1.1, the contact probes are usually used in UT. In this work conventional ultrasonic contact probe is considered. A model developed by Boström and Wirdelius [7] can be used to model incident signal.

The surface of the component is free of traction, except beneath the probe. The traction is derived so that a plane wave is generated, see eq. (2.1) for longitudinal (P) and vertical transverse (SV) wave types, respectively.

$$\mathbf{t} = \begin{cases} Ai\mu k_p \left[ \delta \sin(2\gamma) \mathbf{e}_{x_1^t} + \left( \frac{k_s^2}{k_p^2} - 2 \sin^2(\gamma) \right) \mathbf{e}_{x_2^t} \right] e^{-ik_p x_1^t \sin(\gamma)}, & \text{P probe} \\ Ai\mu k_s \left[ -\delta \cos(2\gamma) \mathbf{e}_{x_1^t} + \sin(2\gamma) \mathbf{e}_{x_2^t} \right] e^{-ik_s x_1^t \sin(\gamma)}, & \text{SV probe} \end{cases} \quad (2.1)$$

where  $\mathbf{e}_{x_1^t}$  and  $\mathbf{e}_{x_2^t}$  are the unit vectors in corresponding directions,  $A$  is the displacement amplitude of the plane wave,  $\mu$  is the Lamé constant of the elastic half space,  $k_p$  and  $k_s$  are longitudinal and transverse wave numbers, respectively.  $\gamma$  is the angle of the probe, measured clockwise from the normal of the probe. Parameter  $\delta$  is used to consider the effect of the couplant applied between the wedge and the scanning surface:  $\delta = 1$  for glued probe and  $\delta = 0$  for fluid coupling, for the fluids with different viscosity parameter could vary as  $0 < \delta < 1$ .

The Fourier transform  $\mathbf{T}^t$  of the prescribed traction  $\mathbf{t}$  is described in the paper by Westlund and Boström [13], and the equation is given as:

$$\mathbf{T}^t = \begin{cases} Ai\mu k_p \left[ \delta \sin(2\gamma) \mathbf{e}_{x_1^t} + \left( \frac{k_s^2}{k_p^2} - 2 \sin^2(\gamma) \right) \mathbf{e}_{x_2^t} \right] \frac{2 \sin(w_t(q + k_p \sin(\gamma)))}{q + k_p \sin(\gamma)}, & \text{P probe} \\ Ai\mu k_s \left[ -\delta \cos(2\gamma) \mathbf{e}_{x_1^t} + \sin(2\gamma) \mathbf{e}_{x_2^t} \right] \frac{2 \sin(w_t(q + k_s \sin(\gamma)))}{q + k_s \sin(\gamma)}, & \text{SV probe} \end{cases} \quad (2.2)$$

where  $w_t$  – half diameter of the transmitting probe and  $q$  - Fourier space variable.

It is convenient to express traction this way, because it will be used later to calculate the incident field.

#### 2.1.4 Statement of the problem

In this work a 2D in-plane scattering problem is considered, see Figure 2.3. A circle shaped cavity, e.g. a side drilled hole, is located in the elastic half-space, which is isotropic and homogeneous with Lamé constants  $\mu$  and  $\lambda$  and density  $\rho$ . On the top of the scanning surface an ultrasonic probe is located. The probe can act as both transmitter and receiver to model a pulse-echo testing situation. Multiple scattering between the scanning surface and the defect is neglected, so the distance between them can be arbitrary, but assumed to be large enough (e.g. at least a couple of wavelengths).

In the Figure 2.3 two coordinate systems are introduced: the probe coordinate system  $x_i^t$  and the cavity coordinate system  $x_i^d$ .

On the surface of the cavity a traction-free (for hollow cavity) boundary condition is used. The scanning surface of the component is also traction-free except for the area beneath the ultrasonic probe (more about the probe model in Section 2.1.3).

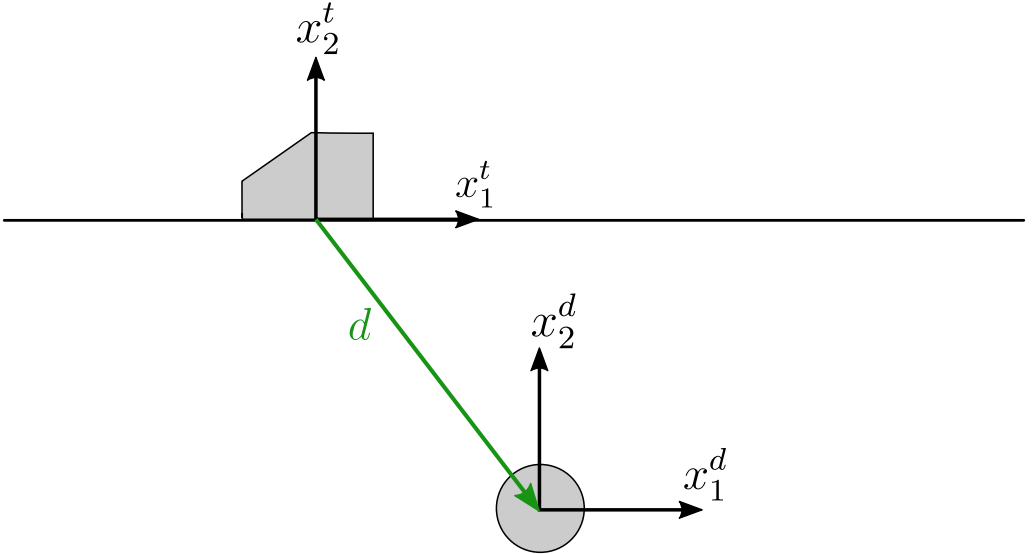


Figure 2.3: *Illustration of the geometry with a defect in the elastic half-space*

## 2.2 Analytical solution

### 2.2.1 Elastic waves

In the analytical solution the propagation of the waves can be described by the elastodynamic equation of motion. If the time-harmonic conditions are assumed, the factor  $e^{-i\omega t}$ , where  $\omega$  is the angular frequency and  $t$  is time, can be suppressed throughout. The equation of motion, where  $\mathbf{u}$  is the displacement field, can be written as:

$$k_p^{-2}\nabla(\nabla \cdot \mathbf{u}) - k_s^{-2}\nabla \times (\nabla \times \mathbf{u}) + \mathbf{u} = \mathbf{0} \quad (2.3)$$

where  $k_p = \frac{\omega}{c_p}$  and  $c_p = \sqrt{\frac{(\lambda+2\mu)}{\rho}}$  are pressure wave number and pressure wave speed, respectively;  $k_s = \frac{\omega}{c_s}$  and  $c_s = \sqrt{\frac{\mu}{\rho}}$  are shear wave number and shear wave speed, respectively.

The total displacement field is considered as a summation of the incident field  $\mathbf{u}^{in}$  and the scattered field  $\mathbf{u}^{sc}$ :

$$\mathbf{u} = \mathbf{u}^{in} + \mathbf{u}^{sc} \quad (2.4)$$

The displacement field can be written as:

$$\mathbf{u} = \nabla\Phi + \nabla \times (\mathbf{e}_z\Psi) \quad (2.5)$$

where the  $\Phi$  and  $\Psi$  are scalar and vector potentials, respectively. Substitution equation (2.5) into the (2.4) will show that potentials satisfy Helmholtz equation with wavenumbers  $k_p$  and  $k_s$ , respectively:

$$\begin{aligned} \nabla^2\Phi + k_p^2\Phi &= 0 \\ \nabla^2\Psi + k_s^2\Psi &= 0 \end{aligned} \quad (2.6)$$

Analytical solution could be done in any coordinate system, and in this case it is more convenient to write down the solution in cylindrical coordinates, as the incoming wave will be scattered from a circle shaped obstacle. By using  $\nabla$  operator for the cylindrical coordinate system as:

$$\nabla = \frac{\partial}{\partial r}\hat{\mathbf{r}} + \frac{1}{r}\frac{\partial}{\partial \varphi}\hat{\boldsymbol{\varphi}} \quad (2.7)$$

and using separation of variables, the potentials  $\Phi$  and  $\Psi$  may be expressed as:

$$\begin{aligned}\Phi^0 &= J_m(k_p r) \begin{pmatrix} \cos(m\varphi) \\ \sin(m\varphi) \end{pmatrix} \\ \Psi^0 &= J_m(k_s r) \begin{pmatrix} \cos(m\varphi) \\ \sin(m\varphi) \end{pmatrix}\end{aligned}\tag{2.8}$$

where the upper index "0" is used for regular waves, containing Bessel functions  $J_m$ . The corresponding outgoing waves have upper index "+" and contain Hankel functions  $H_m^{(1)}$ .

The incident field can be expanded in terms of regular cylindrical vector wave functions ( $\chi_{\tau\sigma m}^0$ ), and the scattered field caused by any obstacles can be expanded in its outgoing cylindrical vector wave functions ( $\chi_{\tau\sigma m}^+$ ):

$$\begin{cases} \mathbf{u}^{in} = \sum_{\tau\sigma m} b_{\tau\sigma m} \chi_{\tau\sigma m}^0 \\ \mathbf{u}^{sc} = \sum_{\tau\sigma m} f_{\tau\sigma m} \chi_{\tau\sigma m}^+ \end{cases}\tag{2.9}$$

Corresponding wave functions could then be defined as:

$$\begin{aligned}\chi_{1\sigma m}^0(\mathbf{r}) &= \frac{\sqrt{\varepsilon_m}}{2} \left[ \mathbf{e}_r \frac{m}{k_s r} J_m(k_s r) \begin{pmatrix} -\sin(m\varphi) \\ \cos(m\varphi) \end{pmatrix} - \mathbf{e}_\varphi J'_m(k_s r) \begin{pmatrix} \cos(m\varphi) \\ \sin(m\varphi) \end{pmatrix} \right] \\ \chi_{2\sigma m}^0(\mathbf{r}) &= \frac{\sqrt{\varepsilon_m} k_p}{2k_s} \left[ \mathbf{e}_r J'_m(k_p r) \begin{pmatrix} \cos(m\varphi) \\ \sin(m\varphi) \end{pmatrix} + \mathbf{e}_\varphi \frac{m}{k_p r} J_m(k_p r) \begin{pmatrix} -\sin(m\varphi) \\ \cos(m\varphi) \end{pmatrix} \right]\end{aligned}\tag{2.10}$$

Here the first index  $\tau = 1$  and  $\tau = 2$  on the wave functions indicates transverse (SV) and longitudinal (P) waves, respectively,  $m = 0, 1, 2, 3, \dots$  and  $\sigma = e$  (even) for the upper row or  $\sigma = o$  (odd) for the lower row, with  $\sigma = o$  excluded for  $m = 0$ . The Neumann factor  $\varepsilon_0 = 1$  and  $\varepsilon_m = 2$  for  $m = 1, 2, 3, \dots$ . The upper index "0" on the wavefunction means that these functions are regular, so the Bessel functions  $J_m$  are used, the corresponding outgoing wavefunctions have the upper index "+" and contain Hankel functions  $H_m^{(1)}$ . As we can see from the equation above, the wave functions have different dependence on  $\varphi$ , cosine and sine functions switched place. For the case of scattering by the circle, it is convenient to couple wave functions in this order:  $\tau = 1$   $\sigma = e$  with  $\tau = 2$   $\sigma = o$  and  $\tau = 1$   $\sigma = o$  with  $\tau = 2$   $\sigma = e$ .

Traction is needed for the applying correct boundary conditions. The corresponding traction on  $r = a$  could be calculated from equation:

$$\begin{aligned}
\mathbf{t}^{(r)}(\chi_{1\sigma m}^0) &= \frac{\mu\sqrt{\varepsilon_m}}{2} \left[ \mathbf{e}_r 2m \frac{d}{dx} \left( \frac{J_m(k_s r)}{k_s r} \right) \begin{pmatrix} -\sin(m\varphi) \\ \cos(m\varphi) \end{pmatrix} - \right. \\
&\quad \left. - \mathbf{e}_\varphi k_s J_m''(k_s r) \begin{pmatrix} \cos(m\varphi) \\ \sin(m\varphi) \end{pmatrix} \right] \\
\mathbf{t}^{(r)}(\chi_{2\sigma m}^0) &= \frac{\mu\sqrt{\varepsilon_m}}{2k_s} \left[ \mathbf{e}_r \left( 2k_p^2 J_m''(k_p r) + (2k_p^2 - k_s^2) J_m(k_p r) \right) \begin{pmatrix} \cos(m\varphi) \\ \sin(m\varphi) \end{pmatrix} + \right. \\
&\quad \left. + \mathbf{e}_\varphi 2mk_p \frac{d}{dx} \left( \frac{J_m(k_p r)}{k_p r} \right) \begin{pmatrix} -\sin(m\varphi) \\ \cos(m\varphi) \end{pmatrix} \right]
\end{aligned} \tag{2.11}$$

Traction for outgoing wave functions can be determined in the same way as for the displacement field by changing all Bessel functions to Hankel functions in (2.11).

### 2.2.2 T matrix

In this work scattering from the circled shaped obstacle with radius  $a$  is considered. Surrounding material is isotropic and homogeneous. The source of the wave is assumed to be located outside the defect, so the plane wave can be considered. The incident wave field can be expanded in terms of regular wave functions:

$$\mathbf{u}^{in}(\mathbf{r}) = \sum_{\tau\sigma m} b_{\tau\sigma m} \chi_{\tau\sigma m}^0(\mathbf{r}) \tag{2.12}$$

where the summation is over  $\tau = 1, 2$ ,  $\sigma = e, o$  and  $m = 0, 1, 2, 3, \dots$ , with  $\sigma = o$  excluded for  $m = 0$ . The expansion coefficients  $b_{\tau\sigma m}$  can be considered as known, as they can be found from the probe and incoming wave configurations. The wave scattered by the defect is considered to carry energy away from the obstacle, and it is possible to expand scattered field in the outgoing wave functions as:

$$\mathbf{u}^{sc}(\mathbf{r}) = \sum_{\tau\sigma m} f_{\tau\sigma m} \chi_{\tau\sigma m}^+(\mathbf{r}) \tag{2.13}$$

Here the expansion coefficients  $f_{\tau\sigma m}$  are unknown. It is possible to determine them with the help of incident wave configuration and the properties of the obstacle. When both these coefficients, for incident and scattered waves, are



calculated, the transition (T) matrix could be determined. This matrix is defined as a linear relation between the expansion coefficients [7]:

$$f_{\tau\sigma m} = \sum_{\tau'\sigma'm'} T_{\tau\sigma m, \tau'\sigma'm'} b_{\tau'\sigma'm'} \quad (2.14)$$

For the circular (homogeneous) obstacle the T matrix could be written as:

$$T_{\tau\sigma m, \tau'\sigma'm'} = \delta_{mm'} \xi_{\tau\sigma, \tau'\sigma'} T_{\tau\tau'}^m \quad (2.15)$$

$$\text{where } \xi_{\tau\sigma m, \tau'\sigma'm'} = \begin{cases} 1 & \text{if } \tau = \tau' \text{ and } \sigma = \sigma' \text{ or } \tau \neq \tau' \text{ and } \sigma \neq \sigma' \\ 0 & \text{otherwise} \end{cases}$$

From the equation above we can see that for our case transition matrix is symmetric and diagonal except that mode coupling elements between P and SV waves are nonzero if the  $m$  values are the same and the  $\sigma$  values are different.

The advantage of calculating T matrix is that it fully describes the obstacle and is independent of the location of the incident wave signal.

### 2.2.3 Expansion coefficients for incoming wave

The incident field (2.2) from the transmitting probe may be analytically solved for in term of a Fourier transform. Using the notation of Boström et. al. [14] for the Fourier transform, the incident field can be written as:

$$\mathbf{u}^{in,t}(\mathbf{x}^t) = \sum_{j=1}^2 \int_{C_-} \xi_j(\beta) \boldsymbol{\varphi}_j^t(\beta; \mathbf{x}^t) d\beta \quad (2.16)$$

where  $\boldsymbol{\varphi}_j$  – vector plane waves and  $j = 1, 2$  corresponds to SV and P waves, respectively,  $\beta$  – is a polar angle of propagation of the plane wave. The vector plane waves could be written as:

$$\begin{aligned} \boldsymbol{\varphi}_1(\beta, \mathbf{x}) &= -\frac{i\hat{\beta}}{8\pi} e^{ik_s \hat{\gamma} \cdot \mathbf{x}}, \\ \boldsymbol{\varphi}_2(\beta, \mathbf{x}) &= \frac{k_p}{k_s} \frac{i\hat{\gamma}}{8\pi} e^{ik_p \hat{\gamma} \cdot \mathbf{x}}, \end{aligned} \quad (2.17)$$

with polar unit vectors:

$$\begin{aligned} \hat{\beta} &= (\cos\beta, \sin\beta) \\ \hat{\gamma} &= (-\sin\beta, \cos\beta) \end{aligned} \quad (2.18)$$

The integration contour  $C_-$  - in this case is defined as  $\beta \in [0, 2\pi]$ , see the Boström et al. [14], where the integration contour is named  $\Gamma_-$ . In order to determine functions  $\xi_j(\beta)$ , it is necessary to transform equation to rectangular coordinate  $q$  in Fourier space. Then, calculate the corresponding traction and identify it with the Fourier transformed traction  $\mathbf{T}^t$  of the prescribed traction from the probe, eq. (2.2). The functions could be written as [9]:

$$\begin{aligned}\xi_1(q) &= \sqrt{\frac{2}{\pi}} \frac{h_s k_s}{\mu R} [(2q^2 - k_s^2) T_1^t - 2h_p q T_2^t] \\ \xi_2(q) &= \sqrt{\frac{2}{\pi}} \frac{h_p k_s}{\mu R} [2h_s q T_1^t + (2q^2 - k_s^2) T_2^t]\end{aligned}\tag{2.19}$$

where  $R = 4q^2 h_p h_s + (2q^2 - k_s^2)^2$  is the Rayleigh function and  $h_j = h_j(q) = \sqrt{k_j^2 - q^2}$  with  $j = p, s$ .  $\mathbf{T}^t$  - the Fourier transform of the prescribed traction, see eq. (2.2). The incident field from the probe can be determined with  $\xi_1(\beta) = \xi_1(q = k_s \cos \beta)$  and  $\xi_2(\beta) = \xi_2(q = k_p \cos \beta)$ .

By transforming the vector plane waves  $\boldsymbol{\varphi}_j$  into the cylindrical vector wave functions  $\chi_{j\sigma m}$  it is possible to determine the expansion coefficients  $b_{j\sigma m}$  in the incoming field equation (2.9). Such transformation could be done in two steps: first, the plane waves should be translated from the center of the probe to an origin at the center of the defect; then, expanded in the cylindrical wave functions. More details of these transformations are described by Boström et al. [14]. In our case, after all transformations, coefficients could be defined as:

$$b_{j\sigma m} = i^m \sqrt{\frac{\varepsilon_m}{2\pi}} \int_{C_-} \xi_j(\beta) e^{ik_j \hat{\gamma} \cdot \mathbf{d}} \begin{pmatrix} \cos(m\beta) \\ \sin(m\beta) \end{pmatrix} d\beta \tag{2.20}$$

where  $\mathbf{d}$  is the vector directed from the center of the probe to the center of the cavity.

## 2.2.4 Expansion coefficients for scattered wave

To simplify the way of using wave function equations and to avoid possible misreading, it is convenient to use such notification of the equation (2.10):

$$\begin{aligned}\chi_{1\sigma m}^0(r) &= \left[ V_{r1m}^0(r) \begin{pmatrix} -\sin(m\varphi) \\ \cos(m\varphi) \end{pmatrix} + V_{\varphi1m}^0(r) \begin{pmatrix} \cos(m\varphi) \\ \sin(m\varphi) \end{pmatrix} \right] \\ \chi_{2\sigma m}^0(r) &= \left[ V_{r2m}^0(r) \begin{pmatrix} \cos(m\varphi) \\ \sin(m\varphi) \end{pmatrix} + V_{\varphi2m}^0(r) \begin{pmatrix} -\sin(m\varphi) \\ \cos(m\varphi) \end{pmatrix} \right]\end{aligned}\tag{2.21}$$

As for the actual equations, the upper index "0" is used for the regular wave functions, and that means, that it is contained Bessel functions. For the outgoing

wave functions index " + " is used, and all Bessel functions are switched to the Hankel functions. Traction equations (2.11) could be transformed in the same way:

$$\begin{aligned} \mathbf{t}^{(r)}(\chi_{1\sigma m}^0) &= \left[ S_{r1m}^0(r) \begin{pmatrix} -\sin(m\varphi) \\ \cos(m\varphi) \end{pmatrix} + S_{\varphi1m}^0(r) \begin{pmatrix} \cos(m\varphi) \\ \sin(m\varphi) \end{pmatrix} \right] \\ \mathbf{t}^{(r)}(\chi_{2\sigma m}^0) &= \left[ S_{r2m}^0(r) \begin{pmatrix} \cos(m\varphi) \\ \sin(m\varphi) \end{pmatrix} + S_{\varphi2m}^0(r) \begin{pmatrix} -\sin(m\varphi) \\ \cos(m\varphi) \end{pmatrix} \right] \end{aligned} \quad (2.22)$$

With such notation of wave functions and traction, analytical solution could be written more clearly. First, the simple case with hollow cavity as a defect is considered. As the boundary condition both traction components are equal to zero. For  $m = 0$  there are some restrictions: for  $\tau = 1$  only an azimuthal traction is considered, and for  $\tau = 2$  – only radial traction component. So, for  $m = 0$  there are no coupling between  $\tau = 1$  and  $\tau = 2$ . The boundary condition at  $r = a$  for  $m = 0$  and  $\tau = 1$  gives:

$$S_{\varphi10}^0(a)b_{1e0} + S_{\varphi10}^+(a)f_{1e0} = 0 \quad (2.23)$$

Similarly, the boundary condition for  $\tau = 2$  gives:

$$S_{r20}^0(a)b_{2e0} + S_{r20}^+(a)f_{2e0} = 0 \quad (2.24)$$

Full boundary condition equations for  $m = 1, 2, 3, \dots$  can be written as:

$$\begin{aligned} S_{r,1m}^0(a)b_{1om} + S_{r,2m}^0(a)b_{2em} + S_{r,1m}^+(a)f_{1om} + S_{r,2m}^+(a)f_{2em} &= 0 \\ S_{\varphi,1m}^0(a)b_{1om} + S_{\varphi,2m}^0(a)b_{2em} + S_{\varphi,1m}^+(a)f_{1om} + S_{\varphi,2m}^+(a)f_{2em} &= 0 \\ S_{r,1m}^0(a)b_{1em} + S_{r,2m}^0(a)b_{2om} + S_{r,1m}^+(a)f_{1em} + S_{r,2m}^+(a)f_{2om} &= 0 \\ S_{\varphi,1m}^0(a)b_{1em} + S_{\varphi,2m}^0(a)b_{2om} + S_{\varphi,1m}^+(a)f_{1em} + S_{\varphi,2m}^+(a)f_{2om} &= 0 \end{aligned} \quad (2.25)$$

The expansion coefficients for scattered wave could be found by solving the system of equations ((2.23), (2.24) and (2.25)) in terms of the incoming wave expansion coefficients (2.20). With both sets of these expansion coefficients known, it is possible to define T matrix, using eq. (2.14) and (2.15) and solving the corresponding system of equation for each value of  $m$ . The final equations are quite big, therefore are not given.

## 3 Numerical solution

### 3.1 Considered software

Any in-service inspection must be performed by using qualified procedures, which are reliable to detect, locate, characterise and accurately determine the size of defects that may occur in the specific type of component. To qualify the procedures a big amount of inspections on the test pieces is a conventional routine, which is very costly and time-consuming. A thoroughly validated model could be used as an alternative or an addition to the experimental work in order to reduce the cost.

There are several options how to model the inspection situation, mostly semi-analytical and numerical approaches are implemented [10]. Using only semi-analytical methods for modeling UT inspection limits the possibilities to model the geometry of the defect. Simple-shaped defects are well defined, and the analytical solution for them are known, or can be easily derived. Hence, most of the time simple-shaped defects, such as spheres, strip-like or penny-shaped cracks, are used to model the real test situations. However, in real life defects are far more complex. Numerical approaches work better for complicated geometry. Although, using numerical based software for modeling a realistic NDT situation, where the distance between the probe and the defect could be large, might be very expensive, because the big amount of computer memory might be required.

The hybrid methods take advantage of both semi-analytical and numerical approaches. The basic idea is to surround the defect by a finite element scheme and use the semi-analytical method for the propagating between the probe and the defect. In this case it is possible to model more complicated shape of the defect, which involves more complicated scattering process without getting too large numerical models.

It is convenient to use already existing software, which is validated to meet all the needed requirements for the task. Further in this section, as in the Paper A, three software are considered.

#### 3.1.1 simSUNDT

The *simSUNDT* software consists of a Windows<sup>®</sup>-based pre- and post-processor, as well as a mathematical kernel *UTDefect* [8, 15] that conducts the actual mathematical modeling and computation. *UTDefect* was developed at Chalmers University of Technology and has been experimentally validated and verified [16, 17]. The 3D elastodynamic wave equation, which defines the wave propagation in a homogeneous half space, is solved using vector wave functions [15].

The modelling of the contact probe assumes that the probe is placed on an elastic half-space. The surface of that half-space is traction free, except the area beneath the probe. This enables an adaptation to a variety of realistic parameters related to the probe, e.g. wave type, angle, crystal (e.g. size and shape), focus depth and contact conditions, etc.

The traction is derived in the manner, that a plane wave is generated in the far field. This approach is used in elastodynamic wave propagation problem, see eq. (2.1) for two dimensional longitudinal (P) and vertical transverse (SV) wave types.

UTDefect uses the T-matrix method [18], and all information regarding the defects is included in the transition matrix, as well as the linear relation between the expansion coefficients of the incoming ( $b_{\tau\sigma m}$ ) and scattered ( $f_{\tau\sigma m}$ ) wave fields in eq. (2.14). To incorporate the probe model into the T-matrix formulation, the displacement field needs to be transformed from the plane vector waves centered at the contact area into spherical vector wave functions oriented and centered at the defect. The receiver is modeled by applying an Auld's reciprocity argument [19]. The electrical signal response is derived in [15] and can be expressed as:

$$\delta\Gamma \sim \sum_{nn'} a_n^b T_{nn'} a_{n'}^a \quad (3.1)$$

where  $a_{n'}^a$  represents transmitting probe,  $T_{nn'}$  - defect and  $a_n^b$  - receiving probe.

### 3.1.2 k-Wave toolbox

*k-Wave* is an open source MATLAB<sup>®</sup> toolbox designed for the time-domain simulation of propagating acoustic waves in 1D, 2D, or 3D [20]. The toolbox is an advanced numerical model that can account for both linear and nonlinear wave propagation and an arbitrary distribution of heterogeneous material parameters [21]. The equations in the toolbox are solved using a k-space pseudospectral method, where spatial gradients are calculated using a Fourier collocation scheme.

The *k-Wave* toolbox was originally developed within the Photoacoustic Imaging Group at University College London (UCL). The first beta version was focused primarily on forward and inverse initial value problems for the simulation and reconstruction of photoacoustic wave fields in lossless media [20]. In the updated version, time varying pressure and velocity sources, acoustic absorption, nonlinearity, elastic materials and models for ultrasound transducers are included in the toolbox.

As the modeling of ultrasound transducers and wave propagation in the toolbox were done mostly for biomedical ultrasonics, it is impossible to use materials with large differences in density in *k-Wave* simulation. Hence, there is a massive

limitation on shape and type of the modelled defects. The other critical limitation in this software is the fact, that the wave numbers depend on the grid, which makes it impossible to apply Fourier transformation and consider the problem in the frequency domain.

### 3.1.3 COMSOL Multiphysics

The COMSOL Multiphysics® software is a simulation platform that includes all of the steps requires in the modeling process: defining geometries, material properties, physics that describe specific phenomena, solving and postprocessing models.

This software allows to combine any physics phenomena from electromagnetics, structural mechanics, acoustics, fluid flow, heat transfer, and chemical reaction phenomena in a single model. Accurate multiphysics models consider a wide range of possible operating conditions and physical effects. This makes it possible to use models for understanding, designing, and optimizing processes and devices for realistic operating conditions.

For each modeling situation software suggests available study types, such as time-dependent or stationary solvers. The software also automatically recommends the appropriate numerical discretization of the mathematical model, solver sequence, and visualization and postprocessing settings that are specific to the physics phenomena. The physics interfaces can also be combined freely in order to describe processes that involve multiple physics phenomena.

The acoustic module works with analysis of acoustics and vibration problems [22]. It is possible to solve problems in linear ultrasound and propagation of pressure and elastic waves in porous materials. In general, the interface of this module is suited for modeling the propagation of acoustic signals over large distances relative to the wavelength. The interface includes absorbing layers that are used to set up effective nonreflecting like boundary conditions. The interface is based on the discontinuous Galerkin (dG or dG-FEM) method and uses a time explicit solver. The method is very memory efficient and can solve problems with many million degrees of freedom (DOFs). However, it is not possible to get a value of the displacement field as an outcome in this module.

The Structural Mechanics Module is more suitable for determination of the displacement field [23]. It solves problems in the fields of structural and solid mechanics, including special physics interfaces for modeling shells and beams. The physics interfaces in this module are fully multiphysics enabled, making it possible to couple them to any other physics interfaces in COMSOL Multiphysics®. Several material models are available, such as: isotropic, orthotropic, or fully anisotropic Linear Elastic Materials, Linear Viscoelastic, Piezoelectric, etc. The

study capabilities include static, eigenfrequency, time dependent (transient), frequency response, buckling, and parametric studies. There is a possibility to do calculations in time or frequency domain, or apply Fourier transformation.

## 3.2 Validation and comparison of the results

### 3.2.1 Paper A

A 2D time-dependent problem was considered in Paper A. The ultrasonic line-source was located on the surface of a half infinite solid structure and modelled as a pressure distribution with values for the specific line. The perfectly matched layer (k-Wave) and low-reflected boundary (COMSOL Multiphysics®) were used to allow a free-field simulation at the borders of the computational grid. A defect was located in the material underneath the probe. Three simple shaped defects were considered in the paper: side-drilled hole (SDH), perpendicular and parallel strip-like cracks (SC). The values of diameter of SDH and length of SC were equal. The distance between the probe and the upper surface of the defect was the same for all three defects. The distribution of the resulting stress field can be seen in Figure 3.1.

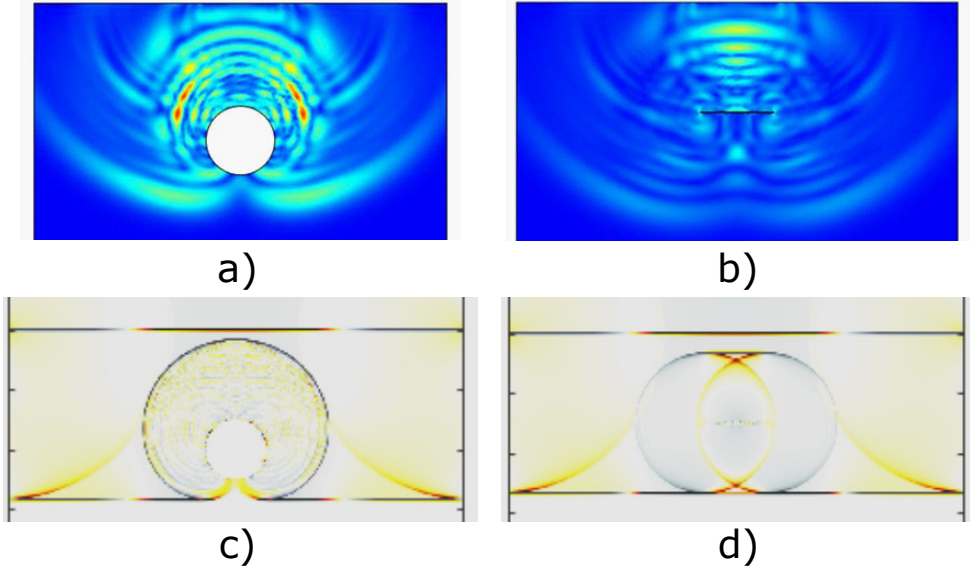


Figure 3.1: *Stress field at  $t=2.9 \mu s$  for SDH and parallel SC in COMSOL Multiphysics® (a, b) and in k-Wave (c, d)*

Even if the stress distribution in the Figure 3.1 looks correct, the actual values

of stress and displacement, calculated in the COMSOL Multiphysics<sup>®</sup>, were very noisy. The reason for this was that in the version 5.4 of the software, which was used in this paper, the low-reflected boundary condition in combination with the prescribed pressure from the probe were not working correctly for the Structural Mechanics Module. The values of the displacement field were much bigger and much noisier, in comparison with other software, thus they were not included on the graphs below. In the later version of COMSOL Multiphysics<sup>®</sup> it becomes possible to include the perfectly matched layer as the boundary condition in the Structural Mechanics Module.

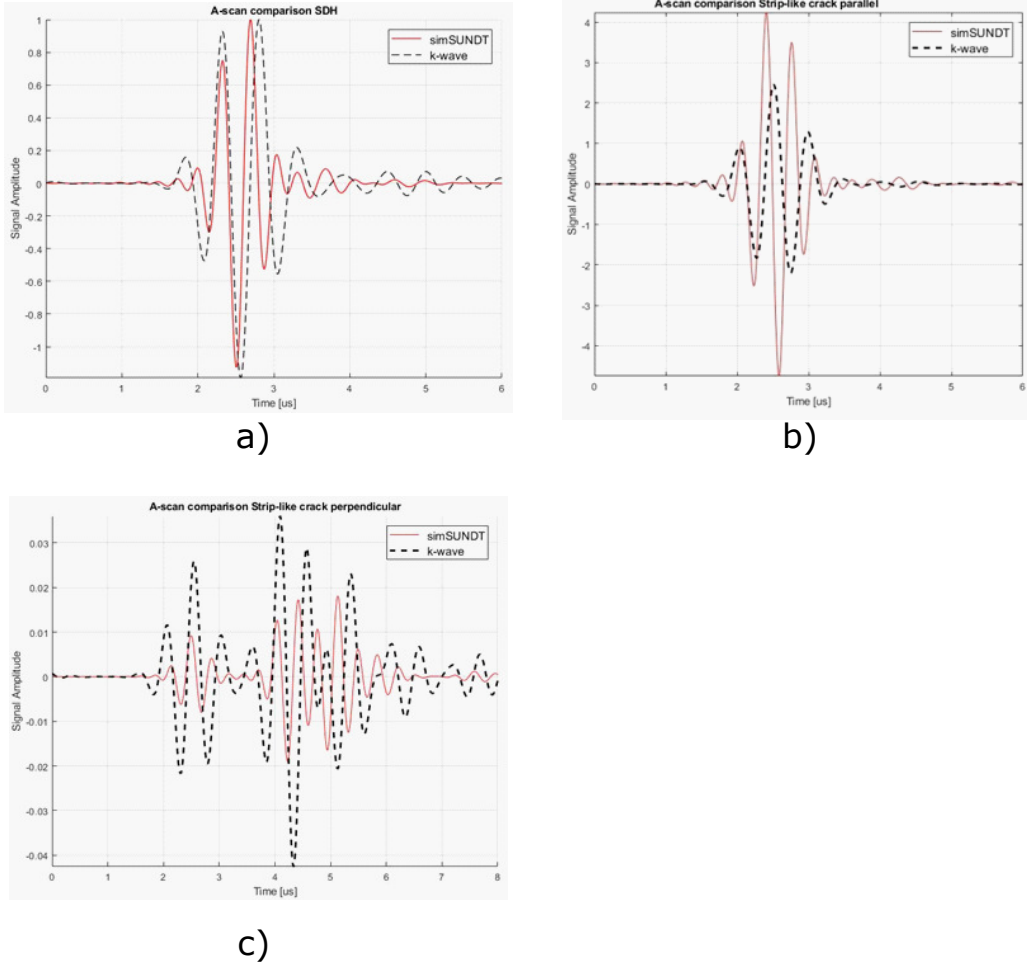


Figure 3.2: Comparison of A-scan for: a) SDH, b) SC parallel, c) SC perpendicular in SimSUNDT and k-Wave



In Figure 3.2 a comparison of the results from simSUNDT and k-Wave is presented. For each defect two simulations were made: with and without defect. It was done in order to be able to compare results with simSUNDT, where the Auld’s reciprocity relation is used to calculate the change in the signal [19]. As a result, only pure signal from the defect was considered, since the signal from the case ‘without defect’ was subtracted. Presented results are normalized to SDH, which means that all values are divided by the maximum value for SDH case.

One of the main limitation in k-Wave is the inability to use materials with large differences in density. Therefore, for the solid structure the properties of steel (density, pressure and shear wave speeds) were used, and for the defects, values of these properties are reduced by 100. In comparison, in SimSUNDT and COMSOL Multiphysics® it is possible to model a void with zero material properties (vacuum).

SC might be modelled as a rectangular crack with very small thickness compare to the length. In the case of a SC parallel to the surface, the thickness does not matter, since the largest amount of received energy is due to reflection from the parallel surface of the defect. The crack-tip diffraction tends to be much smaller than corresponding surface reflection.

For the perpendicular SC case the dimension of crack tip matters. In modeling, the value of the width of the crack tip depends on the mesh. In k-Wave the smallest possible mesh does not allow to neglect the impact of the parallel surface and the corners of the defect. In order to avoid such influence, the crack was modelled as a rigid line with no thickness, instead of rectangular looking one. That is not physically correct, and thus the differences in results seems bigger than in other cases, see Figure 3.2, c).

The agreement between SimSUNDT and k-Wave could be considered quite good, as the position and shape of the signal are very similar, but there are some important limitations which prevent the use of this software for further research. Most essential features that may limit its application in wave propagation are the wavenumber dependence on grid and inability to use materials with large differences in density.

## 4 Hybrid modelling

The hybrid model, as a combination of two different methods, takes advantage of both semi-analytical and numerical approaches. By using such models it becomes possible to consider complex shape defects without describing it analytically, which might be very complicated or even impossible.

The hybrid model is based on using two approaches separately for the specific

parts of the problem first, and then combining them. The analytical method is used for describing the wave propagation between the probe and the defect, and the numerical solution simulates the interaction between the wave and the complex shape defect by surrounding it with a finite element scheme.

In this work, for the analytical part MATLAB<sup>®</sup> software was used. The simulation was done in the Fourier space in cylindrical coordinate system.

The COMSOL Multiphysics<sup>®</sup> software was used for the numerical calculations. The simulations were done in frequency domain using the Structural mechanics Module with the rectangular coordinate system.

## 4.1 Determination of $\mathbf{T}$ matrix

For the geometry, an infinite elastic half-space, see Figure 2.3, was considered. The surface was traction-free except beneath the probe, located on the surface. For the prescribed traction SV probe signal was used, see eq. (2.1). The defect, the hollow cavity in our case, was located underneath the probe in the material.

It is necessary to have similar geometry, material properties, boundary conditions and incoming wave from the probe for analytical and numerical solutions to be able to combine them. Hence, for the boundary condition in COMSOL<sup>®</sup> a perfectly matched layer was used to model an infinite half-space, which allows waves to propagate without being scattered from the boundaries, see Figure 4.1.

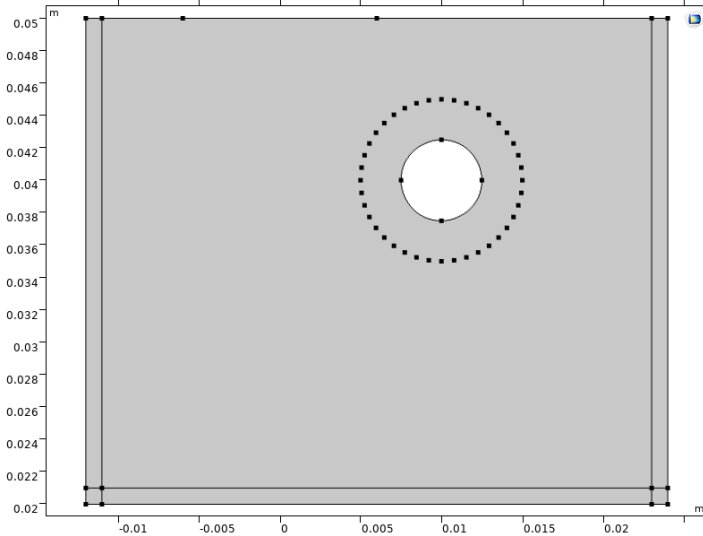


Figure 4.1: Model created in COMSOL Multiphysics<sup>®</sup> version 5.6

In the Figure 4.1 the radius of the outer circle, which surrounds the defect, is twice bigger than the radius  $R$  of the obstacle. This circle consists of points, where the displacement field data from numerical model was collected and used in further calculations of T matrix.

T matrix describes a linear relationship between expansion coefficients for incoming wave  $b_{\tau\sigma m}$  and expansion coefficients for scattered wave  $f_{\tau\sigma m}$ . Equations (2.14) and (2.15) can be used to determine T matrix. As we know, expansion coefficients for incoming wave only depend on the probe configurations, so they can be easily derived using (2.20) for any frequency and  $m$  values.

The situation with expansion coefficients for scattered wave is more complicated. In the analytical solution they could be found by solving the system of equations, described in Section (2.2.4), and using the traction-free boundary conditions on the surface of the hollow cavity. But in the real life situation the boundary conditions of the defect could not be determined. Thus, our hybrid model uses a numerical data received from the COMSOL<sup>®</sup> simulation as an updated boundary conditions.

The boundary conditions and the system of equations could be updated: instead of considering the surface of the defect, where the value of total displacement field is equal to zero, the displacement field on the outer circle should be considered. In that case, we could put the value of total field equal to the values that are collected from the COMSOL<sup>®</sup>. It is important to use the same coordinates of the data points in both analytical and numerical solution to be able to put an equal sign between them. The updated equation for boundary condition can be expressed as:

$$\sum_{\tau\sigma m} (b_{\tau\sigma m} \chi_{\tau\sigma m}^0(r, \varphi) + f_{\tau\sigma m} \chi_{\tau\sigma m}^+(r, \varphi)) = U_{com}(r, \varphi) \quad (4.1)$$

where  $r$  and  $\varphi$  are the coordinates of the considered data point,  $U_{com}(r, \varphi)$  - displacement field in the same point, collected from COMSOL<sup>®</sup>.

The amount of equations in the system depends on the  $m$  value. For each natural  $m$  number there are 4 unknown expansion coefficients  $f_{\tau\sigma m}$ , and for  $m = 0$  with the restrictions, similar to eq. (2.23) and (2.24), there are only two unknown expansion coefficients  $f_{1e0}$  and  $f_{2e0}$ . Both radial and azimuthal components (or x and y components in the rectangular coordinate system) are used in this system of equations.

The expansion coefficients for scattered wave could be found by solving the updated system of equations (4.1) in terms of the incoming wave expansion coefficients  $b_{\tau\sigma m}$ , see eq. (2.20). With both sets of these expansion coefficients known, the T matrix could be defined, using eq. (2.14) and (2.15) for each  $m$  value.

The T matrix contains information about the defect and do not depend on any probe configuration or position. Therefore, with T matrix known it is possible to model a scanning inspection situation for the range of probe positions. To verify the developed model, comparison with numerical results are used.

## 4.2 Validation and comparison results

### 4.2.1 Paper B

Paper B describes the developed hybrid model. In this paper, a 2D in-plane scattering problem was considered, the full description of which could be found in Section 2.

The numerical calculations for the 2D hybrid model were done in COMSOL Multiphysics®. The analytical solution, determination of T matrix and further calculations were done in MATLAB®. *Vpasolve* command was used in MATLAB® to numerically solve the systems of equations and to determine the values of expansion coefficients for incoming and scattered waves.

T matrix was calculated for the *Position 1* of the probe, see Figure 4.2, according to the procedure described in Section 4.1. Probe angle  $\gamma = -\frac{\pi}{4}$  for the *Position 1* was used, in order to get maximum level of scattered energy to use in the T matrix calculations.

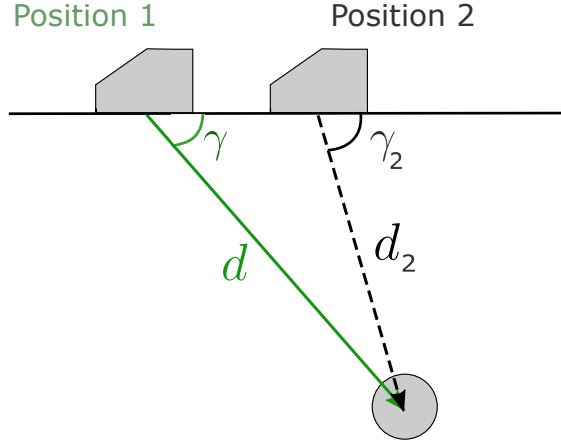


Figure 4.2: *Illustration of the different positions of the probe*

With known T matrix it becomes possible to use it to determine the expansion coefficients for scattered wave, eq. (2.14) and (2.15), for any *Position 2* of the probe, in this work  $\gamma_2 = -\frac{\pi}{6}$ . After that, the displacement field could easily be

calculated.

To verify that the hybrid model is working correctly for any *Position 2* of the probe, the full numerical model was created in COMSOL<sup>®</sup>, and the full analytical model - in MATLAB<sup>®</sup>. Simulations were done separately for each value of the frequency from 1 to 6MHz with  $m$  equal to 9.

To determine the total displacement for each point on the outer circle in COMSOL<sup>®</sup>, the *solid.disp* command was used, the equation for which can be expressed as:

$$solid.disp = \sqrt{real(U_x)^2 + real(U_y)^2} \quad (4.2)$$

where the  $U_x$  and  $U_y$  are the displacement components in the  $x$  and  $y$  directions of the rectangular coordinate system. The displacement components are complex numbers, but only *real* part is used to calculate the total displacement.

In results presented in Figure 4.3 and Figure 4.4, the analytical and hybrid solutions in MATLAB<sup>®</sup> were done in the cylindrical coordinate system. Hence, the determined displacement components  $U_r$  and  $U_\varphi$  should be transformed, see eq. (4.3), into the rectangular coordinates to make it possible to compare results.

$$\begin{aligned} U_x &= U_r \cos(\varphi) - U_\varphi \sin(\varphi) \\ U_y &= U_r \sin(\varphi) + U_\varphi \cos(\varphi) \end{aligned} \quad (4.3)$$

where  $U_x$ ,  $U_y$  and  $U_r$ ,  $U_\varphi$  are displacement field components in rectangular and cylindrical coordinate systems, respectively;  $\varphi$  - angle coordinate.

In this work, two sets of results are presented. The comparison of the total displacement field vs. angle  $\varphi$  on the outer circle for the radius equal to  $2R$  and  $1.05R$  could be found in the Figure 4.3 and Figure 4.4, respectively, where  $R$  is the radius of the obstacle. Calculations were done separately for each frequency from 1 to 6MHz with the step of 1MHz. On the graphs, solid black line represents results from Hybrid model, dotted blue line is assigned for the Numerical solution made in COMSOL<sup>®</sup>, red dash line is used for Analytical solution. All presented values are normalized, so we can compare only the shape of the signal.

The Hybrid solution is located in between the analytical and numerical solutions, as expected. This solution has better correlation with numerical part than the analytical one has.

Comparing results in Figure 4.3 and Figure 4.4, it is obvious that the displacement fields for hybrid and numerical solutions, calculated on the radius  $1.05R$ , have better correlation, than the same calculated on the radius  $2R$ . That might be connected with the numerical values, which were used to determine the T matrix. These data were collected from COMSOL<sup>®</sup> separately for two corresponding

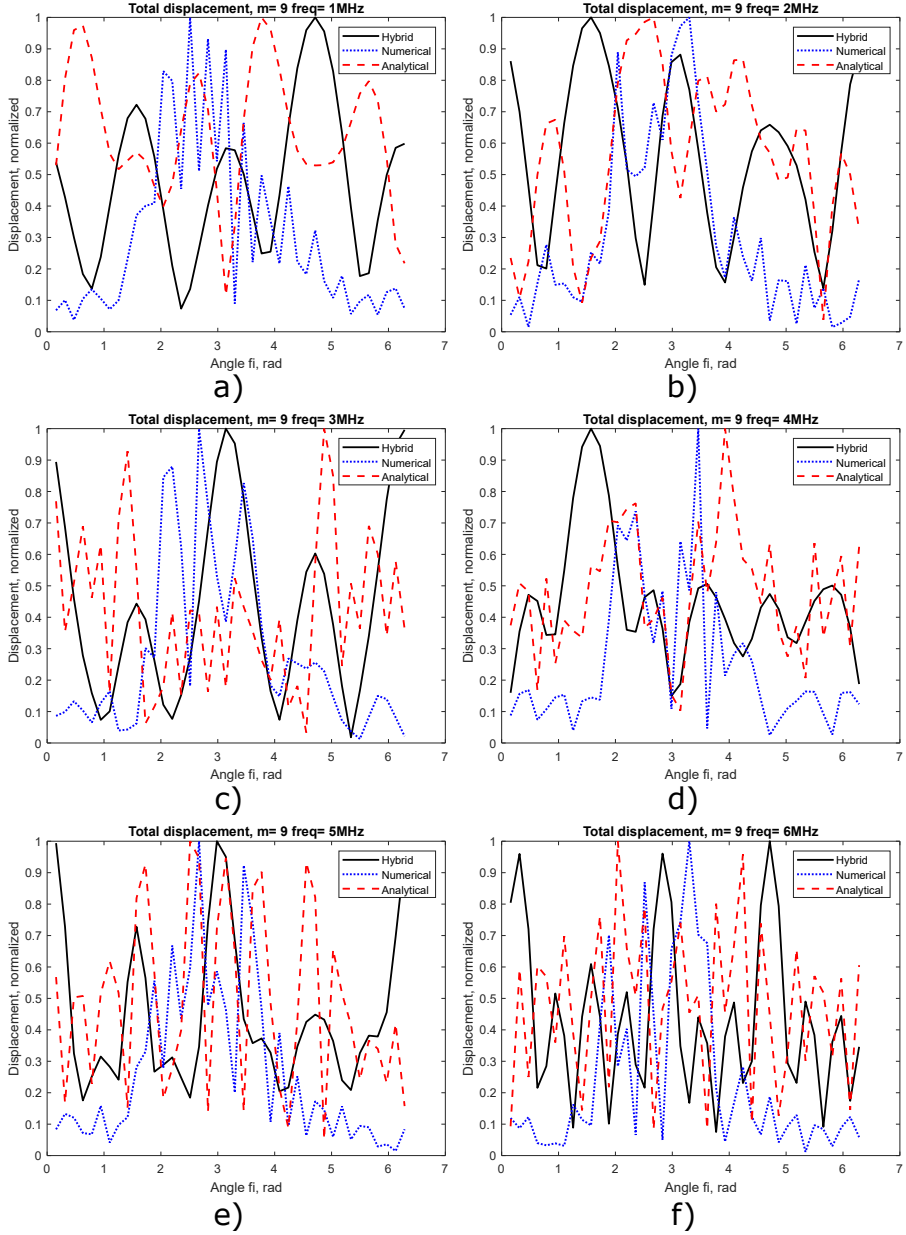


Figure 4.3: Comparison of Hybrid (solid, black), Numerical (dotted, blue) and Analytical (dash, red) solutions for different frequencies with radius of outer circle equal  $2R$

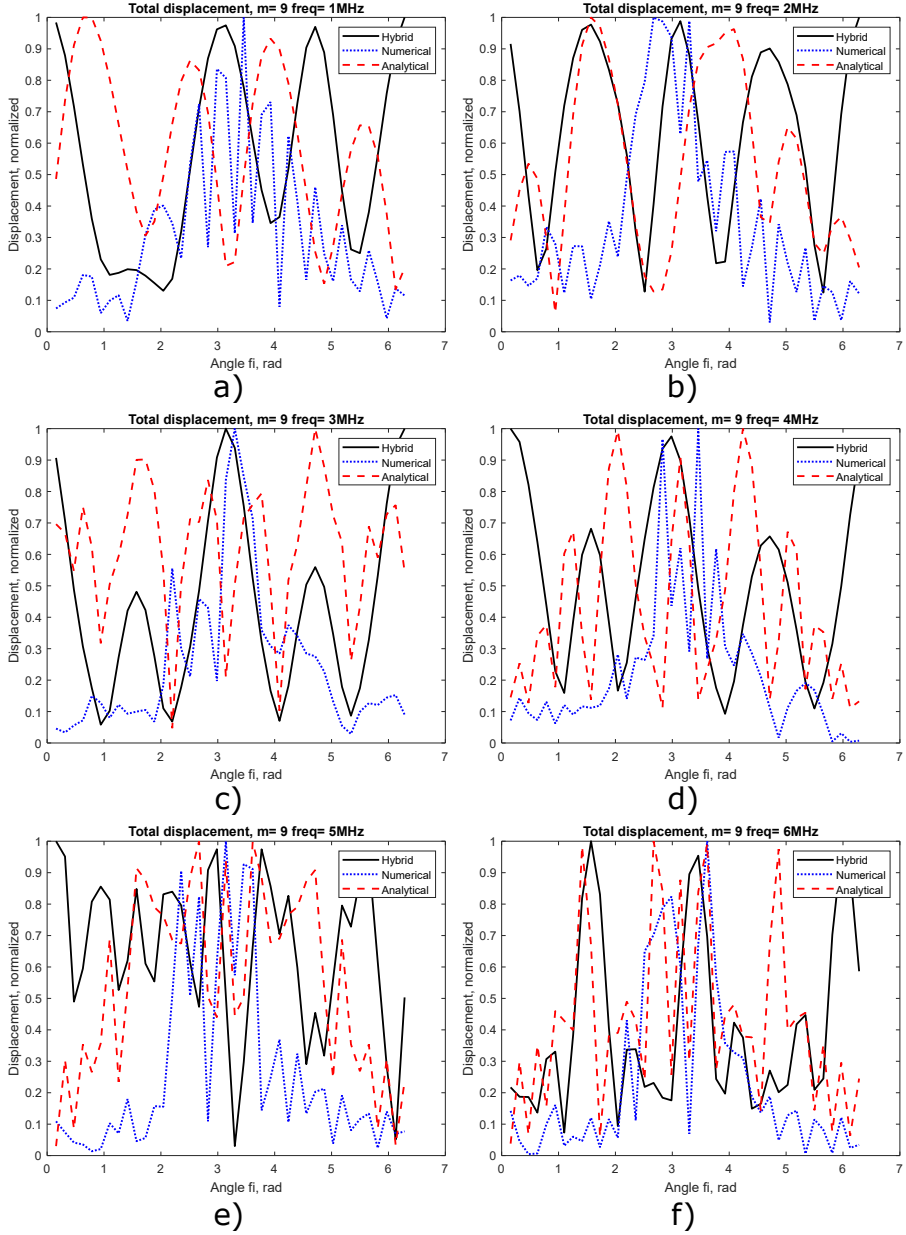


Figure 4.4: Comparison of Hybrid (solid, black), Numerical (dotted, blue) and Analytical (dash, red) solutions for different frequencies with radius of outer circle equal  $1.05R$

values of the outer circle radius. The bigger distance from the actual defect we use to collect the data, the noisier signal we get. Thus, the total result is highly dependent on the fact, which data was used to determine T matrix.

The differences between the solutions for the higher frequencies, Figure 4.4, e)-f), is more noticeable than for the lower frequencies, Figure 4.4, a)-d). The reason for this could be the value  $m$  and the amount of data points used to determine T matrix. In our case,  $m$  was equal 9, thus there were 38 equations used as a boundary condition while calculating T matrix. The amount of equations was divided by 2 to identify how many data points were considered, as both components  $U_x$  and  $U_y$  of the displacement field were used. It might be necessary to have more equations and consider more points to get more accurate results.

In both Figures you can see very big values on the edges of the graphs, around  $\varphi \approx 0$  and  $\varphi \approx 2\pi$ . It might be connected with the sine and cosine functions, that were used for calculating displacement components in the hybrid model equations. That phenomenon should be investigated further.



## 5 Summary of appended papers

### 5.1 Paper A

There are several options how to model the inspection situation, mostly semi-analytical and numerical approaches are implemented. Using only semi-analytical methods for modeling UT inspection limits the possibilities to model the geometry of the defect. Numerical approaches work better for complicated geometry. Although, using numerical based software for modeling a realistic NDT situation might be very expensive and time consuming, because the big amount of computer memory might required. It is more suitable to use the Hybrid model, which combines both semi-analytical and numerical approaches.

To develop the Hybrid model, it is convenient to use already existing numerical software, which is validated to meet all the needed requirements for the task. In Paper A, a 2D time-dependent problem with simple shape defects was simulated in three software: k-Wave toolbox for MATLAB<sup>®</sup>, COMSOL Multiphysics<sup>®</sup> and simSUNDT.

Though, the agreement between the stress and displacement field for all software could be considered quite good, some important limitations, which prevent the use of the software as it is for further research were discovered. One of the main limitation in k-Wave is the inability to use materials with large differences in density. For COMSOL Multiphysics<sup>®</sup> version 5.4, which was used in this paper, the boundary condition in combination with the prescribed pressure from the probe were not working correctly for the Structural Mechanics Module. This problem was solved in the later version, which allow us to use this software for further research.

### 5.2 Paper B

The Hybrid model is based on using semi-analytical and numerical approaches separately for the specific parts of the problem first, and then combining them. The analytical method is used for describing the wave propagation between the probe and the defect, and the numerical solution simulates the interaction between the wave and the complex shape defect by surrounding it with a finite element scheme. In this Paper, the numerical calculations for the 2D hybrid model were done in COMSOL Multiphysics<sup>®</sup>. The analytical solution, determination of T matrix and further calculations were done in MATLAB<sup>®</sup>.

The developed hybrid model is based on the T matrix method. The T matrix contains information about the defect and do not depend on any probe config-

uration or position. Therefore, with  $T$  matrix known it is possible to model a scanning inspection situation for the range of frequencies and probe positions. To verify the developed model, comparison with fully numerical and fully analytical results were used. Simulations were done separately for several values of the frequency.

## 6 Conclusion and future plans

In recent years, the problem of the power plants being exploited beyond their estimated lifetimes in combination with an increase of power outage is very urgent. In-service caused defects can, if they are detected, be sized and monitored in order to postpone repairs or replacements.

Stress corrosion cracks (SCC) and fatigue cracks are the most common defects that appeared in the nuclear industry. SCC tends to have a heavily branched macroscopic shape with a large number of crack tips. The diffraction from the cracks tips is used as the basis for the defect size analysis, and ultrasonic NDT methods are not always reliable in in this kind of application. In this case, mathematical modelling could be used to do the parametrical studies that address such interactions and dependencies that never would be possible to achieve by experiments.

In this thesis, a newly developed hybrid model is described. This model is based on using semi-analytical and numerical approaches separately for the specific parts of the problem first, and then combining them. The analytical method is used for describing the wave propagation between the probe and the defect, and the numerical solution simulates the interaction between the wave and the complex shape defect by surrounding it with a finite element scheme. The numerical calculations for the 2D hybrid model were done in COMSOL Multiphysics®. The analytical solution, determination of T matrix and further calculations were done in MATLAB®.

The Hybrid model is using T matrix method to combine two approaches. The T matrix contains information about the defect and do not depend on probe configuration or position. Therefore, with T matrix known it is possible to model a scanning inspection situation for the range of probe positions. To verify the developed model, comparison with fully numerical and fully analytical results were used. Simulations were done separately for several values of the frequency.

The comparison of the results from Hybrid, Numerical and Analytical solutions is shown to have good agreement in general. The Hybrid solution is located in between the analytical and numerical solutions, as expected. This solution has better correlation with numerical part than the analytical one has.

Based on the results, the next step of the research is investigation of possibility to validated this model with more complex defects, such as SCC or defects surrounded by strongly anisotropic material. The further development of the Hybrid model into the 3D case is look like the natural continuation of the research.

# References

- [1] Peter J. Shull. *Nondestructive evaluation: theory, techniques, and applications*. CRC press, 2002.
- [2] R. K. Chapman. A system model for the ultrasonic inspection of smooth planar cracks. *J Nondestruct Eval* **9** (1990), 197–210.
- [3] P. Fellingner et al. Numerical modeling of elastic wave propagation and scattering with EFIT—elastodynamic finite integration technique. *Wave motion* **21.1** (1995), 47–66.
- [4] A. Lhémy et al. Modeling Tools for Ultrasonic Inspection of Welds. *NDT E International* **33** (2000), 499–513.
- [5] J. N. Gray et al. *Metals Handbook* **17** (1989), 202.
- [6] J. D. Achenbach. *Evaluation of Materials and Structures by Quantitative Ultrasonics*. Springer, Wien, 1993.
- [7] A. Boström and H. Wirdelius. Ultrasonic probe modelling and nondestructive crack detection. *The Journal of the Acoustical Society of America* **97.5** (1995), 2836–2848.
- [8] P. Bøvik and A. Boström. A model of ultrasonic nondestructive testing for internal and subsurface cracks. *The Journal of the Acoustical Society of America* **102.5** (1997), 2723–2733.
- [9] J. Westlund and A. Boström. A Hybrid T Matrix/Boundary Element Method for Elastic Wave Scattering from a Defect Near a Non-planar Surface. *Journal of nondestructive evaluation* **31.2** (2012), 148–156.
- [10] A. Jonas Niklasson and Gert Persson. *2005:08 Scattering of SH Waves by Isolated Cracks Using a Hybrid Approach*. SKI report 2005:08. Scientific and Technical Research Reports. Swedish Nuclear Power Inspectorate, SKI, 2005.
- [11] P. Ekström and J. Wåle. *1995:70 Crack characterisation for In-service*. SKI report 1995:70. Scientific and Technical Research Reports. Swedish Nuclear Power Inspectorate, SKI, 1995.
- [12] J. D. Achenbach. *Wave propagation in elastic solids, North-Holland series in applied mathematics and mechanics, v. 16*. Amsterdam, North-Holland Pub. Co.; New York, American Elsevier Pub. Co., 1975.
- [13] J. Westlund and A. Boström. A 2D model of ultrasonic testing for cracks near a non-planar surface. *Wave Motion* **47.6** (2010), 383–394.
- [14] A. Boström, G. Kristensson, and S. Ström. Transformation properties of plane, spherical and cylindrical scalar and vector wave functions. In: V.V Varadan, A. Lakhtakia, V.K. Varadan (eds) *Field Representations and*

- Introduction to Scattering. *Acoustic, Electromagnetic and Elastic Wave Scattering* **1** (1991), 165–210.
- [15] A. Boström and H. Wirdelius. Ultrasonic probe modeling and nondestructive crack detection. *The Journal of the Acoustical Society of America* **97.5** (1995), 2836–2848.
  - [16] J. Niklasson, A. Boström, and H. Wirdelius. *2006:30 Benchmarking - a validation of UTDefect. SKI Report 2006:30*. Scientific and Technical Research Reports. Swedish Nuclear Power Inspectorate, SKI, 2006.
  - [17] H. Wirdelius. “Experimental Validation of the UTDefect Simulation Software”. *Proceedings of 6th International Conference on NDE in Relation to Structural Integrity for Nuclear and Pressurized Components*. 2007.
  - [18] H. Wirdelius. Probe model implementation in the null field approach to crack scattering. *Journal of nondestructive evaluation* **11.1** (1992), 29–39.
  - [19] B. A. Auld. General electromechanical reciprocity relations applied to the calculation of elastic wave scattering coefficients. *Wave motion* **1.1** (1979), 3–10.
  - [20] B. E. Treeby, E. Bradley, and B. T. Cox. k-Wave: MATLAB toolbox for the simulation and reconstruction of photoacoustic wave fields. *Journal of biomedical optics* **15.2** (2010), 021314. URL: <https://doi.org/10.1117/1.3360308>.
  - [21] B. E. Treeby et al. Modeling nonlinear ultrasound propagation in heterogeneous media with power law absorption using a k-space pseudospectral method. *J Acoust Soc Am.* **131.6** (2012), 4324–36. URL: <https://doi.org/10.1117/1.3360308>.
  - [22] COMSOL. *Acoustics Module User’s Guide*. URL: <https://doc.comsol.com/5.4/doc/com.comsol.help.aco/AcousticsModuleUsersGuide.pdf> (visited on 2018).
  - [23] COMSOL. *Structural Mechanics Module User’s Guide*. URL: <https://doc.comsol.com/5.4/doc/com.comsol.help.sme/StructuralMechanics%20ModuleUsersGuide.pdf> (visited on 2018).



Part II  
Appended Papers A–B





# Paper A

Comparison between three mathematical models of three well defined ultrasonic NDT cases



PAPER • OPEN ACCESS

## Comparison between three mathematical models of three well defined ultrasonic NDT cases

To cite this article: M Semenova *et al* 2020 *IOP Conf. Ser.: Mater. Sci. Eng.* **747** 012061

View the [article online](#) for updates and enhancements.

# Comparison between three mathematical models of three well defined ultrasonic NDT cases

**M Semenova, H Wirdelius and G Persson**

Department of Industrial and materials science, Chalmers University of Technology, SE-41296 Gothenburg, Sweden

semenova@chalmers.se

**Abstract.** Ultrasonic nondestructive testing (NDT) is commonly used for in-service inspection in different areas. But reliability of NDT method is highly dependent on the equipment and crack features. Although, it is possible to use thoroughly validated mathematical models to avoid complicated and costly experimental work, when it is necessary to qualify new procedures. Finite Element Model (FEM) is a powerful tool, which is commonly used for such cases. In this paper three mathematical models of three well defined cases will be compared with each other.

## Introduction

The propagation and scattering of waves in the elastic solids are important in ultrasound testing and material characterization. Ultrasonic nondestructive testing (NDT) is commonly used for in-service inspection in different areas, e.g. in nuclear and aerospace industries. NDT methods are used to evaluate the integrity of individual components, which might be exposed to different degradation mechanisms (such as fatigue, corrosion and stress corrosion cracking).

However, the reliability of NDT method is highly dependent on how the equipment is adjusted to a specific object and how to anticipate crack features. Their morphology and thus signal response may vary widely between different crack mechanisms and material types, in which crack appear. Due to these reasons it is very complicated and costly to validate (or qualify) new procedures to inspect defects with more complex geometry, e.g. stress corrosion cracks. Such experimental work requires tests on manufactured specimens with well known fabricated defects.

To avoid these difficulties, it is possible to use thoroughly validated mathematical models. Finite Element Model (FEM) is a powerful and comprehensive tool, which is commonly used nowadays. Up to this date only a couple of models have been developed that cover the whole testing procedure, i.e. they include the modeling of transmitting and receiving probes, the scattering by defects and the calibration. Chapman [1] employs geometrical theory of diffraction for some simple crack shapes and Fellinger et al [2] have developed a type of finite integration technique for a two-dimensional treatment of various types of defects. Lh  mery et al [3] employs Kirchhoff's diffraction theory that enables their model to handle more complex geometries in 3D. In the literature, Gray et al [4] and Achenbach [5] presents overviews of ultrasonic NDT models.

In this paper an ultrasonic "pulse-echo" inspection situation was modelled by a line-shaped source on the surface of a component. Different defects were introduced beneath the source and the signal response from two FEM models and an analytical model were compared.



### Analytical model

The simSUNDT program consists of a windows based pre-processor and postprocessor together with a mathematical kernel (UTDefect) dealing with the actual mathematical modelling. The UTDefect computer code has been developed at Chalmers University of Technology and has been experimentally validated and verified. The analytical model used as kernel in the simSUNDT software [6-8] is completely three dimensional, though the component is two dimensional (infinite plate with finite or infinite thickness) bounded by the scanning surface where one or two probes are scanning the object within a rectangular mesh. The probe is modeled by an assumed effective area beneath the probe, used as boundary conditions in a half-space elastodynamic wave propagation problem. This enables an adaptation to a variety of realistic parameters related to the probe, e.g. wave type, angle, crystal (i.e. size and shape), focus depth and contact conditions. The receiver is modeled by applying a reciprocity argument by Auld [9].

The governing linearized equations for wave propagation in an elastic medium are the equation of motion, Hooke's law and the strain-displacement relation. If time harmonic conditions are assumed (time factor  $e^{-i\omega t}$  is suppressed) these three relations can be combined into the elastodynamic equation of motion governing the displacement field  $\mathbf{u}$ :

$$k_p^{-2} \nabla \nabla \cdot \mathbf{u} - k_s^{-2} \nabla \times \nabla \times \mathbf{u} + \mathbf{u} = \mathbf{0} \quad (1)$$

where  $k_p$  and  $k_s$  are the compressional and shear wave numbers, respectively.

The total displacement field is given by the sum of the incident field ( $\mathbf{u}^i$ ) and the scattered field ( $\mathbf{u}^s$ ). Let us expand the incident field in terms of regular spherical partial vector waves ( $\text{Re}\Psi_n$ ) and the scattered field in corresponding outgoing spherical partial vector waves ( $\Psi_n$ ), i.e.

$$\begin{cases} \mathbf{u}^i = \sum_n a_n \text{Re} \Psi_n \\ \mathbf{u}^s = \sum_n f_n \Psi_n \end{cases} \quad (2)$$

Then it is possible to find a linear relationship between the expansion coefficients for the incident and scattered field and this entity is known as the transition matrix  $T$

$$f_n = \sum_{n'} T_{nn'} a_{n'} \quad (3)$$

All information about the scattered field is contained in its transition matrix and the characterization of the probe acting as a transmitter is encapsulated in the expansion coefficients for the incident field ( $a_n$ ). To evaluate its behaviour as a receiver we use an electromechanical reciprocity argument by Auld [9]. Then the change in the electrical response of probe b, due to the presence of a defect (enclosed by a control surface  $S$ ), is found as

$$\delta\Gamma \sim \sum_{nn'} a_n^b T_{nn'} a_{n'}^a \quad (4)$$

### Numerical models

The discrete modeling is made by using two different approaches, FE-modeling by use of COMSOL and a finite difference method by k-Wave.

COMSOL Multiphysics is a simulation software for a wide array of applications, which included several modules, categorized according to the applications areas: Electrical, Mechanical, Fluid, Chemical, Multipurpose, and Interfacing.

k-Wave is an open source acoustics toolbox for MATLAB and C++. The software is designed for time domain acoustic and ultrasound simulations in complex and tissue-realistic media [10,11]. The equations are solved using a k-space pseudospectral method, where spatial gradients are calculated using a Fourier collocation scheme, and temporal gradients are calculated using a k-space corrected finite-difference scheme.

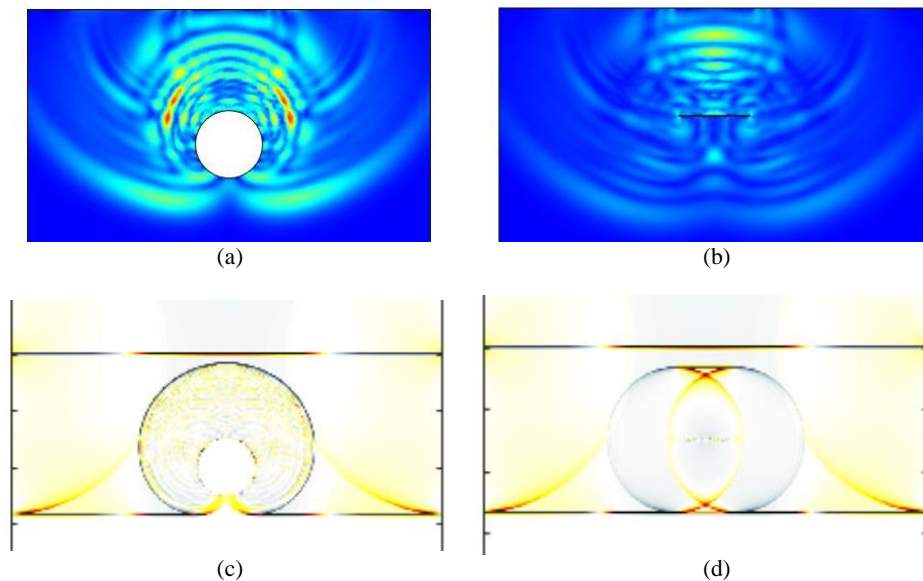


Figure 1. Stress field at  $t=2.9 \mu\text{s}$  for SDH and parallel SC in COMSOL (a, b) and in k-wave (c, d)

In this paper a 2D time-dependent problem is considered. For the geometry, a half infinite solid structure with a defect is used. The perfectly matched layer (k-wave) and low-reflected boundary (COMSOL) are used to allow a free-field simulation at the borders of the computational grid. The ultrasonic 6 mm line-source with a center frequency of 2MHz and 50% bandwidth is placed on the surface and modelled as a pressure distribution with values for specific line. For the defects side-drilled hole (SDH), perpendicular and parallel strip-like cracks (SC) are considered. The diameter of SDH and length of SC are 5 mm, and the distance between probe and the defect is 7,5mm. The resulting stress field can be seen in Figure 1.

In Figure 2 a comparison of the results from simSundt and k-wave is presented. For each defect two simulations are made: with and without defect. As a result, only pure signal from the defect is used, since the signal from the case ‘without defect’ is subtracted. It should be considered, that presented results are normalized to SDH, which means that all values are divided by the maximum value for SDH case.

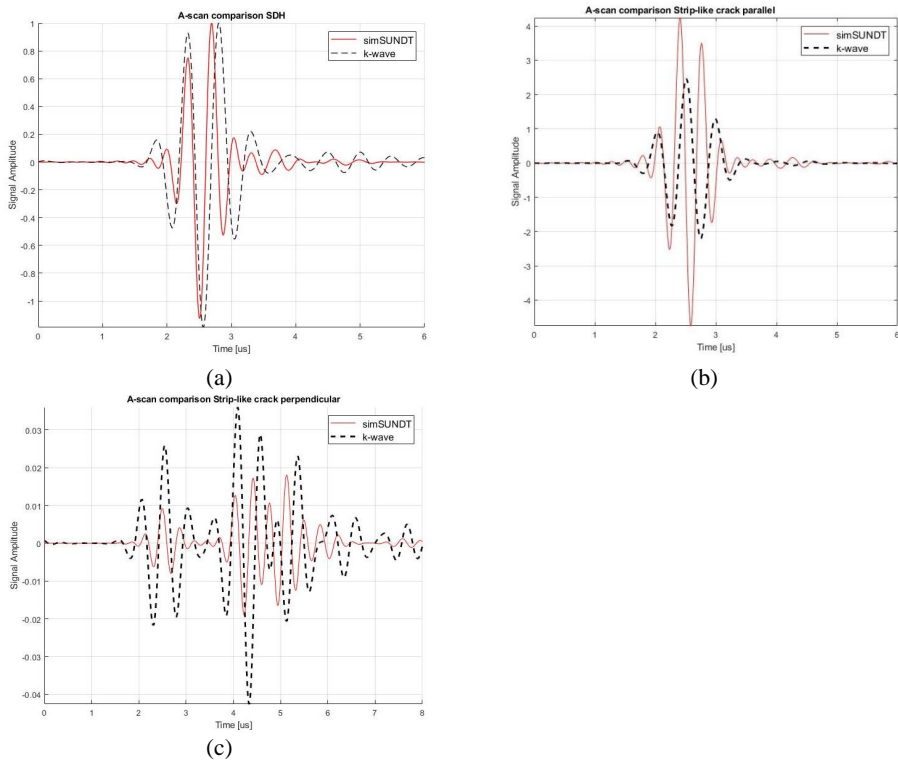


Figure 2. Comparison of A-scan for: (a) SDH, (b) SC parallel, (c) SC perpendicular in SimSUNDT and k-wave

## Results

In k-wave simulation it is impossible to use materials with large differences in density. Hence, properties of steel (density, pressure and shear wave speeds) is used for the solid structure, and for the defects values of these properties are reduced by 100. In comparison, in SimSUNDT and COMSOL it is possible to have a void with zero material properties.

SC might be modelled as a rectangular crack with very small thickness compare to the length. In the case of a SC parallel to the surface, the thickness does not matter, since the largest amount of received energy is due to reflection from the parallel surface of the defect. A rule of thumb is that crack-tip diffraction tends to be about 20 to 30 dB less than corresponding surface reflection.

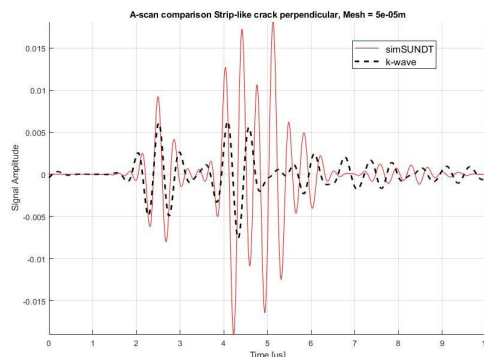


Figure 3. Comparison of A-scan for perpendicular SC in SimSUNDT and perpendicular rectangular SC in k-wave

For the perpendicular SC case the dimension of crack tip is important. In k-wave smallest possible mesh, element size  $50\mu\text{m}$  is used. Accordingly, the smallest possible width of the perpendicular SC is also  $50\mu\text{m}$ . In this case the impact of the parallel surface and the corners of the defect is significant. In Figure 3 you can see that the signal from rectangular SC in k-wave looks like signal from the parallel SC. To avoid this influence, instead of rectangular looking crack there is used a line, located on the grid points under the centre of the probe. That is not physically correct, and thus the differences in results seems bigger than in other cases, see Figure 2, c). However, the agreement between analytical and simulation results in SimSUNDT and k-wave can be considered quite good, as the position and shape of the signal are same, and differences in values are less than 10 dB. Although even if this software has good correlation with analytical solution, there are some features, which may limit further use. One essential parameter that may limit its application in wave propagation is the wavenumber dependence on grid coordinates.

COMSOL results differ a lot from other software. Even if the stress distribution on the pictures looks correct, see Figure 1, the values of stress and displacement are very noisy. Such simulations require big CPU of the computer to be able to use finest mesh and relatively small time-step. However, the good-looking animation of stress distribution can be achieved even with the fine-sized mesh.

## Conclusions

The next step of the research is investigation of possibility to model complexed shaped defects (SCC) or defects surrounded by strongly anisotropic material using existing FEM software. This paper describes a comparison between analytical and two numerical solutions for a 2D time-dependent problem. Both mathematical models have advantages and disadvantages, which must be considered for each simulation purpose.

## Acknowledgements

The present work is financially supported by the Swedish Radiation Safety Authority (SSM) and this is gratefully acknowledged.

## References

- [1] Chapman R K 1990, A System Model for the Ultrasonic Inspection of Smooth Planar Cracks, *J. Nondestr.*



- Eval.* **9**, pp 197-211
- [2] Fellinger P, Marklein R, Langenberg K J and Klaholz S 1995, Numerical Modelling of Elastic Wave Propagation and Scattering with EFIT-Elastodynamic Finite Integration Technique, *Wave Motion* **21**, pp 47-66
  - [3] Lhémery A, Calmon P, Levær-Taïbi I, Raillon R and Paradis L 2000, Modeling Tools for Ultrasonic Inspection of Welds, *NDT & E International* **33**, pp 499-513
  - [4] Gray J N, Gray T A, Nakagawa N and Thompson R B 1989 *Metals Handbook* **17** ASM International, Metals Park, Ohio, p 202
  - [5] Achenbach J D 1993, *Evaluation of Materials and Structures by Quantitative Ultrasonics*, Springer, Wien
  - [6] Boström A and Wirdelius H 1995, Ultrasonic probe modeling and nondestructive crack detection, *J. Acoust. Soc. Am.* **97**, pp 2836 – 48
  - [7] Wirdelius H 1995, User Guide to SUND, *Swedish Nuclear Power Inspectorate Report* 00:29, Stockholm
  - [8] Bövik P and Boström A 1997, A model of ultrasonic nondestructive testing for internal and subsurface cracks, *J. Acoust. Soc. Am.* **102**, pp 2723 – 33
  - [9] Auld B A 1979, General electromechanical reciprocity relations applied to the calculation of elastic wave scattering coefficients, *Wave Motion* **1**, pp 3-10
  - [10] Treeby B E, Jaros J, Rohrbach D and Cox B T 2014, Modelling elastic wave propagation using the k-Wave MATLAB toolbox, *Int. Ultrasonics Symp.*, pp. 146-149
  - [11] Treeby B E and Cox B T 2010, Modeling power law absorption and dispersion for acoustic propagation using the fractional Laplacian, *J. Acoust. Soc. Am.* **127**, no. **5**, pp 2741-48



# Paper B

**Parametrical study in hybrid modeling of an ultrasonic inspection situation**



# Parametrical study in hybrid modeling of an ultrasonic inspection situation

Maria Semenova<sup>1</sup>, Håkan Wirdelius<sup>2</sup>

- 1- Department of Industrial and Materials science, Chalmers University of Technology, SE-412 96, Gothenburg, Sweden
- 2- Division of Subtractive and Additive Manufacturing, University West, S- 461 32, Trollhättan, Sweden

## Abstract

In many industrial applications, e.g. nuclear and aerospace industries, components could be exposed to different degradation mechanisms (e. g. fatigue, corrosion, stress corrosion cracking), which might cause defects such as fatigue and stress corrosion cracks. Advanced methods of nondestructive evaluations (NDE) are widely used for in-service inspection to estimate the size of the defect and monitor it over the time in order to postpone repairs or replacements.

The reliability of NDE methods and the interaction between applied energy and addressed defect is highly dependent on the equipment adjustment to a specific object and to the expectation of the crack features. The crack feature and morphology vary widely between different crack mechanisms and between material types, in which crack appears.

In many cases, fatigue and stress corrosion cracks (SCC), as defects with a complex shape, are difficult to characterize with ultrasonic NDE methods. SCC tends to have a heavily branched macroscopic shape with a large number of crack tips. Ultrasonic NDE method is not always reliable in sizing such defects, as the diffraction from the crack tips is commonly used as the basis for such analysis. But a thoroughly validated mathematical models could be used to do the parametrical studies that address such interactions.

The most convenient approach in this case would be to use the hybrid method, which is a combination of a semi-analytical model with a numerical approach. The basic idea of combining these two methods is to use the numerical solution for interaction between the wave and the complex shape defect. This is then done by surrounding it with a volume modelled by a finite element scheme and to use the analytical method for describing the wave propagation between the probe and the volume that contains the actual defect. By using hybrid models for parametrical study, it is possible to avoid costly and time-consuming experimental work.

**Keywords:** T matrix, Finite element method, Modelling, Scattering, Ultrasonics

## 1. Introduction

Nowadays, advanced methods of nondestructive evaluation (NDE) and nondestructive testing (NDT) are commonly used for in-service inspection in many areas, such as nuclear and aerospace industries. NDE could be used to determine and locate flaws and leaks, to estimate chemical composition, mechanical and physical properties of the material, to verify and control processing (e. g. heat treating). Individual components might be exposed to different degradation mechanisms (e. g. fatigue, corrosion, stress corrosion cracking), and NDE could be used to evaluate their integrity.

In-service induced defects, such as fatigue or stress corrosion cracks, appeared in the machinery parts during operation need to be detected, sized and monitored, in order to postpone the repairs or replacement. Such defects become more and more essential to address as the power plants are exploited beyond their estimated lifetimes in combination with an increase of power outage in recent years. NDE methods are commonly used in the industry for that purpose.

The reliability of NDT methods is highly dependent on the equipment adjustment to a specific object and to the expectation of the crack features. The crack feature and morphology vary widely between different crack mechanisms and between material types, in which crack appears. Since all these NDT methods are indirect and based on prior information on signal into the component, some kind of interpretation of received signal is always the basis for judgment of the quality of the component. The different degradation mechanisms produce very different kind of cracks or defects in a 3-D morphological perspective. Therefore, they interact and influence the received signal in an individual manner.

Stress corrosion cracks (SCC) and fatigue cracks are the most common and critical defects that appeared in the nuclear industry. SCC tends to have a heavily branched macroscopic shape with a large number of crack tips. The diffraction from the cracks tips is used as the basis for the defect size analysis, and ultrasonic NDT methods are not always reliable in in this kind of application. In this case, mathematical modelling could be used to do the parametrical studies that address such interactions and dependencies that never would be possible to achieve by experiments.

Instead of costly and complicated experiments, a thoroughly validated mathematical models can be used. Such models are very useful in development of parametric studies and in the qualification of testing procedures. However, up to this date only a couple of models have been developed that cover the whole testing procedure, i.e. they include the modeling of transmitting and receiving probes, the scattering by defects and the calibration. Chapman [1] employs geometrical theory of diffraction for some simple crack shapes and Fellinger et al [2] have developed a type of finite integration technique for a two-dimensional treatment of various types of defects. Lhémy et al [3] employs Kirchhoff's diffraction theory that enables their model to handle more complex geometries in 3D. In the literature, Gray et al [4] and Achenbach [5] presents overviews of ultrasonic NDT models. Boström and Wirdelius [6] presented a model based on the T matrix concept, in principle without any approximation, see e. g. Bøvik and Boström [7] for similar work for cracks. However, it is limited to address

only simple shaped defects. In Westlund and Boström [8] a 2D hybrid model of a defect near the back surface is deduced.

Mathematical modelling of NDT techniques is also essential when it comes to quantifying the capacity of a specific procedure and technique (NDE) in a specific application. A fundamental problem with modelling in-service induced cracks is that each defect is individual with a unique morphology created by a unique stress and chemical environmental progress. Since these specific features of such cracks cannot be prescribed without a large amount of uncertainty, the conventional way to model these cracks is to generalize into a very simplified and idealized geometric shape.

The hybrid method takes advantage of both semi-analytical and numerical approaches. The basic idea is to surround the defect by a finite element scheme and deal with the propagation between the probe and the defect with a semi analytical method. In this way it is possible to model more complex crack geometries that involves a complicated scattering processes without getting to large numerical models. Where it is possible to implement, semi-analytical and fully numerical approaches are complementary.

## 2. Statement of the problem

In this paper a 2D in-plane scattering problem is considered, see Figure 1. A circle shaped cavity is located in the elastic half-space, which is isotropic and homogeneous with Lamé constants  $\mu$  and  $\lambda$  and density  $\rho$ . On the top of the scanning surface an ultrasonic probe is located. The probe can act as both transmitter and receiver to model a pulse-echo testing situation. Multiple scattering between the scanning surface and the defect is neglected, so the distance between them can be arbitrary, but assumed to be large enough (i.e. at least a couple of wavelengths).

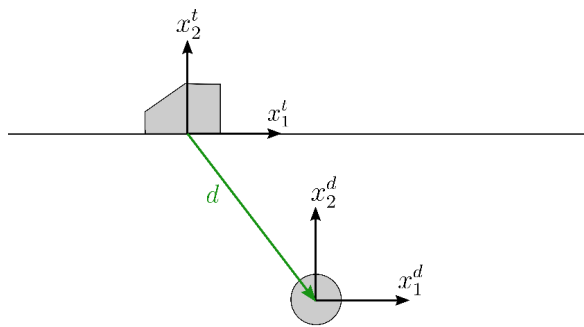


*Fig. 1. Illustration of the geometry with a defect in the elastic half-space*

In the Figure 1 two coordinate systems are introduced: the probe coordinate system  $x_t^t$  and the cavity coordinate system  $x_t^d$ .

On the surface of the cavity a traction-free (for hollow cavity) boundary condition is used. The scanning surface of the component is also traction-free except for the area beneath the ultrasonic probe, which will be described later.

In the analytical solution the propagation of the waves can be described by the elastodynamic equation of motion. If the time-harmonic conditions are assumed, the factor  $e^{-i\omega t}$ , where  $\omega$  is the angular frequency and  $t$  is time, can be suppressed throughout. The equation of motion, where  $\mathbf{u}$  is the displacement field, can be written as:

$$k_p^{-2} \nabla (\nabla \cdot \mathbf{u}) - k_s^{-2} \nabla \times (\nabla \times \mathbf{u}) + \mathbf{u} = \mathbf{0} \quad (2.1)$$

where  $k_p = \omega/c_p$  and  $c_p = \sqrt{(\lambda + 2\mu)/\rho}$  are pressure wave number and pressure wave speed, respectively;  $k_s = \omega/c_s$  and  $c_s = \sqrt{\mu/\rho}$  are shear wave number and shear wave speed, respectively.

### 3. T matrix method

The total displacement field is considered as a summation of the incident field  $\mathbf{u}^{in}$  and the scattered field  $\mathbf{u}^{sc}$ :

$$\mathbf{u} = \mathbf{u}^{in} + \mathbf{u}^{sc} \quad (3.1)$$

The incident field can be expanded in terms of regular cylindrical vector wave functions  $\chi_{1\sigma m}^0$ , and the scattered field caused by any obstacles can be expanded in its outgoing cylindrical vector wave functions  $\chi_{1\sigma m}^+$  [9]:

$$\begin{cases} \mathbf{u}^{in} = \sum_n b_n \chi_n^0 \\ \mathbf{u}^{sc} = \sum_n f_n \chi_n^+ \end{cases} \quad (3.2)$$

Corresponding wave functions could be defined as:

$$\begin{aligned} \chi_{1\sigma m}^0(\mathbf{r}) &= \frac{\sqrt{\varepsilon_m}}{2} \left[ \mathbf{e}_r \frac{m}{k_s r} J_m(k_s r) \begin{pmatrix} -\sin(m\varphi) \\ \cos(m\varphi) \end{pmatrix} - \mathbf{e}_\varphi J'_m(k_s r) \begin{pmatrix} \cos(m\varphi) \\ \sin(m\varphi) \end{pmatrix} \right] \\ \chi_{2\sigma m}^0(\mathbf{r}) &= \frac{\sqrt{\varepsilon_m} k_p}{2k_s} \left[ \mathbf{e}_r J'_m(k_p r) \begin{pmatrix} \cos(m\varphi) \\ \sin(m\varphi) \end{pmatrix} + \mathbf{e}_\varphi \frac{m}{k_p r} J_m(k_p r) \begin{pmatrix} -\sin(m\varphi) \\ \cos(m\varphi) \end{pmatrix} \right] \end{aligned} \quad (3.3)$$

Here the first index  $\tau = 1$  and  $\tau = 2$  on the wave functions indicates transverse (SV) and longitudinal (P) waves, respectively,  $m = 0, 1, 2, 3 \dots$  and  $\sigma = e$  (even) for the upper row or



$\sigma = o$  (odd) for the lower row, with  $\sigma = o$  excluded for  $m = 0$ . The Neumann factor  $\varepsilon_0 = 1$  and  $\varepsilon_m = 2$  for  $m = 1, 2, 3 \dots$ . The upper index "0" on the wavefunction means that these functions are regular, so the Bessel functions  $J_m$  are used, the corresponding outgoing wavefunctions have the upper index "+" and contain Hankel functions  $H_m^{(1)}$ .

As we can see from the equation above, the wave functions have different dependence on  $\varphi$ , cosine and sine functions switched place. For the case of scattering by the circle, it is convenient to couple wave functions in this order:  $\tau = 1, \sigma = e$  with  $\tau = 2, \sigma = o$  and  $\tau = 1, \sigma = o$  with  $\tau = 2, \sigma = e$ .

Corresponding traction on  $r = a$  will be used as the boundary condition, and could be calculated from equation:

$$\begin{aligned} t^{(r)}(\chi_{1\sigma m}^0) &= \frac{\mu\sqrt{\varepsilon_m}}{2} \left[ e_r 2m \frac{d}{dx} \left( \frac{J_m(k_s r)}{k_s r} \right) \begin{pmatrix} -\sin(m\varphi) \\ \cos(m\varphi) \end{pmatrix} - \right. \\ &\quad \left. - e_\varphi k_s J_m''(k_s r) \begin{pmatrix} \cos(m\varphi) \\ \sin(m\varphi) \end{pmatrix} \right] \\ t^{(r)}(\chi_{2\sigma m}^0) &= \frac{\mu\sqrt{\varepsilon_m}}{2k_s} \left[ e_r (2k_p^2 J_m''(k_p r) + (2k_p^2 - k_s^2) J_m(k_p r)) \begin{pmatrix} \cos(m\varphi) \\ \sin(m\varphi) \end{pmatrix} + \right. \\ &\quad \left. + e_\varphi 2mk_p \frac{d}{dx} \left( \frac{J_m(k_p r)}{k_p r} \right) \begin{pmatrix} -\sin(m\varphi) \\ \cos(m\varphi) \end{pmatrix} \right] \end{aligned} \quad (3.4)$$

In this work scattering from the circled shaped obstacle with radius  $a$  is considered. Surrounding material is isotropic and homogeneous. The source of the wave is assumed to be located outside the defect, so the plane wave can be considered.

The expansion coefficients for incoming wave  $b_{\tau\sigma m}$ , can be considered as known, as they can be found from the probe and incoming wave configurations. The wave scattered by the defect is considered to carry energy away from the obstacle, and the expansion coefficients  $f_{\tau\sigma m}$  for scattered wave are unknown. It is possible to determine them with the help of incident wave configuration and the properties of the obstacle.

When both these sets of coefficients, for incident and scattered waves, are calculated, the transition (T) matrix could be determined. This matrix is defined as a linear relation between the expansion coefficients:

$$f_{\tau\sigma m} = \sum_{\tau'\sigma'm'} T_{\tau\sigma m, \tau'\sigma'm'} b_{\tau'\sigma'm'} \quad (3.5)$$

For the circular (homogeneous) obstacle the T matrix could be written as:

$$T_{\tau\sigma m, \tau'\sigma'm'} = \delta_{mm'} \xi_{\tau\sigma, \tau'\sigma'} T_{\tau\tau'}^m \quad (3.6)$$

where

$$\xi_{\tau\sigma m, \tau'\sigma' m'} = \begin{cases} 1 & \text{if } \tau = \tau' \text{ and } \sigma = \sigma' \text{ or } \tau \neq \tau' \text{ and } \sigma \neq \sigma' \\ 0 & \text{otherwise} \end{cases} \quad (3.7)$$

The advantage of calculating T matrix is that it fully describes the obstacle and is independent of the incident wave.

#### 4. The probe model

In this paper conventional ultrasonic contact probe is considered. A model developed by Boström and Wirdelius [6] can be used to model incident signal.

The surface of the component is free of traction, except beneath the probe. The traction is derived so that a plane wave is generated, see eq. (4.1) for longitudinal (P) and vertical transverse (SV) wave types, respectively.

$$\mathbf{t} = \begin{cases} Ai\mu k_p \left[ \delta \sin(2\gamma) \mathbf{e}_{x_1^t} + \left( \frac{k_s^2}{k_p^2} - 2 \sin^2(\gamma) \right) \mathbf{e}_{x_2^t} \right] e^{-ik_p x_1^t \sin(\gamma)}, & \text{P probe} \\ Ai\mu k_s \left[ -\delta \cos(2\gamma) \mathbf{e}_{x_1^t} + \sin(2\gamma) \mathbf{e}_{x_2^t} \right] e^{-ik_s x_1^t \sin(\gamma)}, & \text{SV probe} \end{cases} \quad (4.1)$$

where  $\mathbf{e}_{x_1^t}$  and  $\mathbf{e}_{x_2^t}$  are the unit vectors in corresponding directions,  $A$  is the displacement amplitude of the plane wave,  $\mu$  is the Lamé constant of the elastic half space,  $k_p$  and  $k_s$  are longitudinal and transverse wave numbers, respectively.  $\gamma$  is the angle of the probe, measured clockwise from the normal of the probe. Parameter  $\delta$  is used to consider the effect of the couplant applied between the wedge and the scanning surface:  $\delta = 1$  for glued probe and  $\delta = 0$  for fluid coupling, for the fluids with different viscosity parameter could vary as  $0 < \delta < 1$ .

The Fourier transform  $\mathbf{T}^t$  of the prescribed traction  $\mathbf{t}$  is described in the paper by Westlund and Boström [10], and the equation is given as:

$$\mathbf{T}^t = \begin{cases} Ai\mu k_p \left[ \delta \sin(2\gamma) \mathbf{e}_{x_1^t} + \left( \frac{k_s^2}{k_p^2} - 2 \sin^2(\gamma) \right) \mathbf{e}_{x_2^t} \right] \frac{2 \sin(w_t(q + k_p \sin(\gamma)))}{q + k_p \sin(\gamma)}, & \text{P probe} \\ Ai\mu k_s \left[ -\delta \cos(2\gamma) \mathbf{e}_{x_1^t} + \sin(2\gamma) \mathbf{e}_{x_2^t} \right] \frac{2 \sin(w_t(q + k_s \sin(\gamma)))}{q + k_s \sin(\gamma)}, & \text{SV probe} \end{cases} \quad (4.2)$$

where  $w_t$  – half diameter of the transmitting probe and  $q$  – Fourier space variable.

The incident field (4.2) from the transmitting probe may be analytically solved for in term of a Fourier transform. Using the notation of Boström et. al. [9] for the Fourier transform, the incident field can be written as:

$$\mathbf{u}^{in,t}(\mathbf{x}^t) = \sum_{j=1}^2 \int_{C_-} \xi_j(\beta) \boldsymbol{\varphi}_j^t(\beta; \mathbf{x}^t) d\beta \quad (4.3)$$

where  $\boldsymbol{\varphi}_j$  – vector plane waves and  $j = 1, 2$  corresponds to SV and P waves, respectively;  $\beta$  – is a polar angle of propagation of the plane wave. The vector plane waves could be written as:

$$\begin{aligned} \boldsymbol{\varphi}_1(\beta, \mathbf{x}) &= -\frac{i\hat{\beta}}{8\pi} e^{ik_s \hat{\gamma} \cdot \mathbf{x}}, \\ \boldsymbol{\varphi}_2(\beta, \mathbf{x}) &= \frac{k_p}{k_s} \frac{i\hat{\gamma}}{8\pi} e^{ik_p \hat{\gamma} \cdot \mathbf{x}}, \end{aligned} \quad (4.4)$$

with polar unit vectors:

$$\begin{aligned} \hat{\beta} &= (\cos\beta, \sin\beta) \\ \hat{\gamma} &= (-\sin\beta, \cos\beta) \end{aligned} \quad (4.5)$$

The integration contour  $C_-$  - in this case is defined as  $\beta \in [0, 2\pi]$ , see the Boström et al. [9], where the integration contour is named  $\Gamma_-$ . In order to determine functions  $\xi_j(\beta)$ , it is necessary to transform equation to rectangular coordinate  $q$  in Fourier space. Then, calculate the corresponding traction and identify it with the Fourier transformed traction  $T^t$  of the prescribed traction from the probe, eq. (4.2). The functions could be written as:

$$\begin{aligned} \xi_1(q) &= \sqrt{\frac{2}{\pi}} \frac{h_p k_s}{\mu R} [(2q^2 - k_s^2) T_1^t - 2h_p q T_2^t] \\ \xi_2(q) &= \sqrt{\frac{2}{\pi}} \frac{h_p k_s}{\mu R} [2h_s q T_1^t + (2q^2 - k_s^2) T_2^t] \end{aligned} \quad (4.6)$$

where  $R = 4q^2 h_p h_s + (2q^2 - k_s^2)^2$  is the Rayleigh function and  $h_j = h_j(q) = \sqrt{k_j^2 - q^2}$  with  $j = p, s$ .  $T^t$  - the Fourier transform of the prescribed traction, see eq. (4.2). The incident field from the probe can be determined with  $\xi_1(\beta) = \xi_1(q = k_s \cos(\beta))$  and  $\xi_2(\beta) = \xi_2(q = k_p \cos(\beta))$ .

By transforming the vector plane waves  $\boldsymbol{\varphi}_j$  into the cylindrical vector wave functions  $\chi_n$  it is possible to determine the expansion coefficients  $b_{\tau\sigma m}$  in the incoming field equation (3.2). Such transformation could be done in two steps: first, the plane waves should be translated from the center of the probe to an origin at the center of the defect; then, expanded in the cylindrical wave functions. More details of these transformations are described by Boström et al. [9]. In our case, after all transformations, coefficients could be defined as:

$$b_{jm\sigma} = i^m \sqrt{\frac{\varepsilon_m}{2\pi}} \int_{C_-} \xi_j(\beta) e^{ik_j \hat{\gamma} \cdot \mathbf{d}} \begin{pmatrix} \cos(m\beta) \\ \sin(m\beta) \end{pmatrix} d\beta \quad (4.7)$$

where  $\mathbf{d}$  vector directed from the center of the probe to the center of the cavity, see Figure 1.

## 5. Hybrid model and Results

The hybrid model is based on using two approaches separately for the specific parts of the problem first, and then combining them. The analytical method is used for describing the wave propagation between the probe and the defect, and the numerical solution simulates the interaction between the wave and the complex shape defect by surrounding it with a finite element scheme. In this paper, for the analytical part MATLAB® software was used. The simulation was done in the Fourier space in cylindrical coordinate system. The COMSOL Multiphysics® software was used for the numerical calculations. The simulations were done in frequency domain using the Structural mechanics Module with the rectangular coordinate system.

It is necessary to have similar geometry, material properties, boundary conditions and incoming wave from the probe to be able to combine these two solutions. Hence, for the boundary condition in COMSOL® a perfectly matched layer was used to model an infinite half-space, which allows waves to propagate without being scattered from the boundaries.

To verify that the hybrid model is working correctly the full model was created in COMSOL®. The diameter of the circle, which surrounds the defect, is twice bigger than the diameter of the obstacle. This circle consists of points, where the displacement field data from numerical model was collected.

The combination of the analytical and numerical approaches was done by calculating the T matrix, by using equations (3.5) and (3.6).

T matrix describes a linear relationship between expansion coefficients for incoming wave  $b_{\tau\sigma m}$  and expansion coefficients for scattered wave  $f_{\tau\sigma m}$ . As we know, expansion coefficients for incoming wave only depend on the probe configurations, so they can be easily derived using (4.7) for any frequency and  $m$  values.

The situation with expansion coefficients for scattered wave is more complicated. In the analytical solution they could be found by using traction - free boundary conditions on the surface of the cavity. But in our model, we need to have these values for the outer circle, which surrounds the defect. The data received from the COMSOL® simulation could help with this issue.

The system of equations for boundary conditions should be updated: instead of having displacement field equal to zero (boundary condition on the surface of the defect) we could put it equal to the values that are collected from the outer circle from the COMSOL®

calculations. In this case, it is important to use the same coordinates of the data point in both analytical and numerical solution to be able to put an equal sign between them. The updated system of equations, with the restrictions for  $m = 0$  included, can be expressed as:

$$\sum_{\tau, m, \sigma} (b_{\tau, m, \sigma} \chi_{\tau, \sigma, m}^0(r, \varphi) + f_{\tau, m, \sigma} \chi_{\tau, \sigma, m}^+(r, \varphi)) = U_{com}(r, \varphi) \quad (5.1)$$

where  $r$  and  $\varphi$  are the coordinates of the considered data point,  $U_{com}(r, \varphi)$  - displacement field in the same point, collected from COMSOL®.

The amount of equations in the system depends on the  $m$  value. For each natural  $m$  number there are 4 unknown expansion coefficients  $f_{\tau\sigma m}$ , and for  $m = 0$  values with  $\sigma = 0$  are excluded, so there are only two unknown expansion coefficients  $f_{1e0}$  and  $f_{2e0}$ . Both radial and azimuthal components (or  $x$  and  $y$  components in the rectangular coordinate system) are used in this system of equations.

The expansion coefficients for scattered wave could be found by solving the updated system of equations, see eq. (5.1) in terms of the incoming wave expansion coefficients  $b_{\tau\sigma m}$ , see eq. (4.7). With both sets of these expansion coefficients known, the T matrix could be defined, using eq. (3.5) and (3.6) for each  $m$  value.

The T matrix contains information about the defect and do not depend on any probe configuration or position. Therefore, with T matrix known it is possible to model a scanning inspection situation for the range of frequencies and probe positions. To verify the developed model, comparison with numerical results is used. Simulations were done separately for each value of the frequency from 1MHz to 6MHz with  $m = 7$ .

T matrix was calculated for the Position 1 of the probe, see Figure 2, with probe angle  $\gamma = \frac{\pi}{4}$ . With known T matrix it becomes possible to use it to determine the expansion coefficients for scattered wave for a new Position 2 of the probe. After that, the displacement field could be easily calculated.

The numerical simulations in COMSOL were done in the rectangular coordinate system. The analytical and hybrid solutions in MATLAB® were done in the cylindrical coordinate system. Hence, the determined displacement components  $U_r$  and  $U_\varphi$  should be transformed into the rectangular coordinates, see eq. (5.2), to make it possible to compare results.

$$\begin{aligned} U_x &= U_r \cos(\varphi) - U_\varphi \sin(\varphi) \\ U_y &= U_r \sin(\varphi) + U_\varphi \cos(\varphi) \end{aligned} \quad (5.2)$$

In the Figure 3 the comparison of the total displacement field vs. angle  $\varphi$  on the outer circle for the three models are presented. Calculations were done separately for each frequency from 1MHz to 6MHz with the step of 1MHz. On the graphs, solid black line represents results from Hybrid model, dotted blue line is assigned for the Numerical solution made in COMSOL®,

red dash line is used for Analytical solution. All presented values are normalized, so we can compare only the shape of the signal.

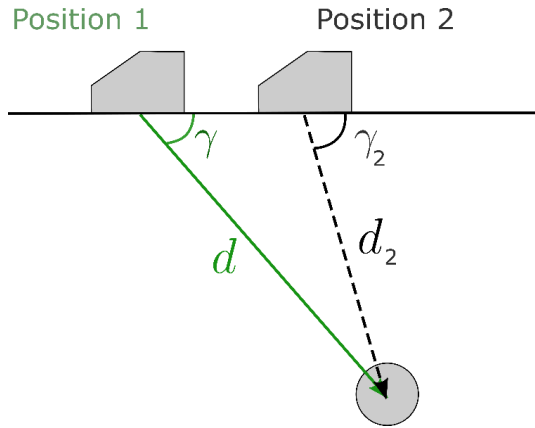


*Fig. 2. Illustration of the different positions of the probe*

The Hybrid solution is located in between the analytical and numerical solutions, as expected. This solution has better correlation with numerical part than the analytical one has.

Comparing results in Figure 3 and Figure 4, it is obvious that the displacement fields for hybrid and numerical solutions, calculated on the radius  $1.05R$ , have better correlation, than the same calculated on the radius  $2R$ . That might be connected with the numerical values, which were used to determine the T matrix. These data were collected from COMSOL® separately for two corresponding values of the outer circle radius. The bigger distance from the actual defect we use to collect the data, the noisier signal we get. Thus, the total result is highly dependent on the fact, which data was used to determine T matrix.

The differences between the solutions for the higher frequencies, Figure 4, e)-f), is more noticeable than for the lower frequencies, Figure 4, a)-d). The reason for this could be the value  $m$  and the amount of data points used to determine T matrix. In our case,  $m$  was equal 9, thus there were 38 equations used as a boundary condition while calculating T matrix. The amount of equations was divided by 2 to identify how many data points were considered, as both components  $U_x$  and  $U_y$  of the displacement field were used. It might be necessary to have more equations and consider more points to get more accurate results.

In both Figures you can see very big values on the edges of the graphs, around  $\varphi \approx 0$  and  $\varphi \approx 2\pi$ . It might be connected with the sine and cosine functions, that were used for calculating displacement components in the hybrid model equations. That phenomenon should be investigated further.

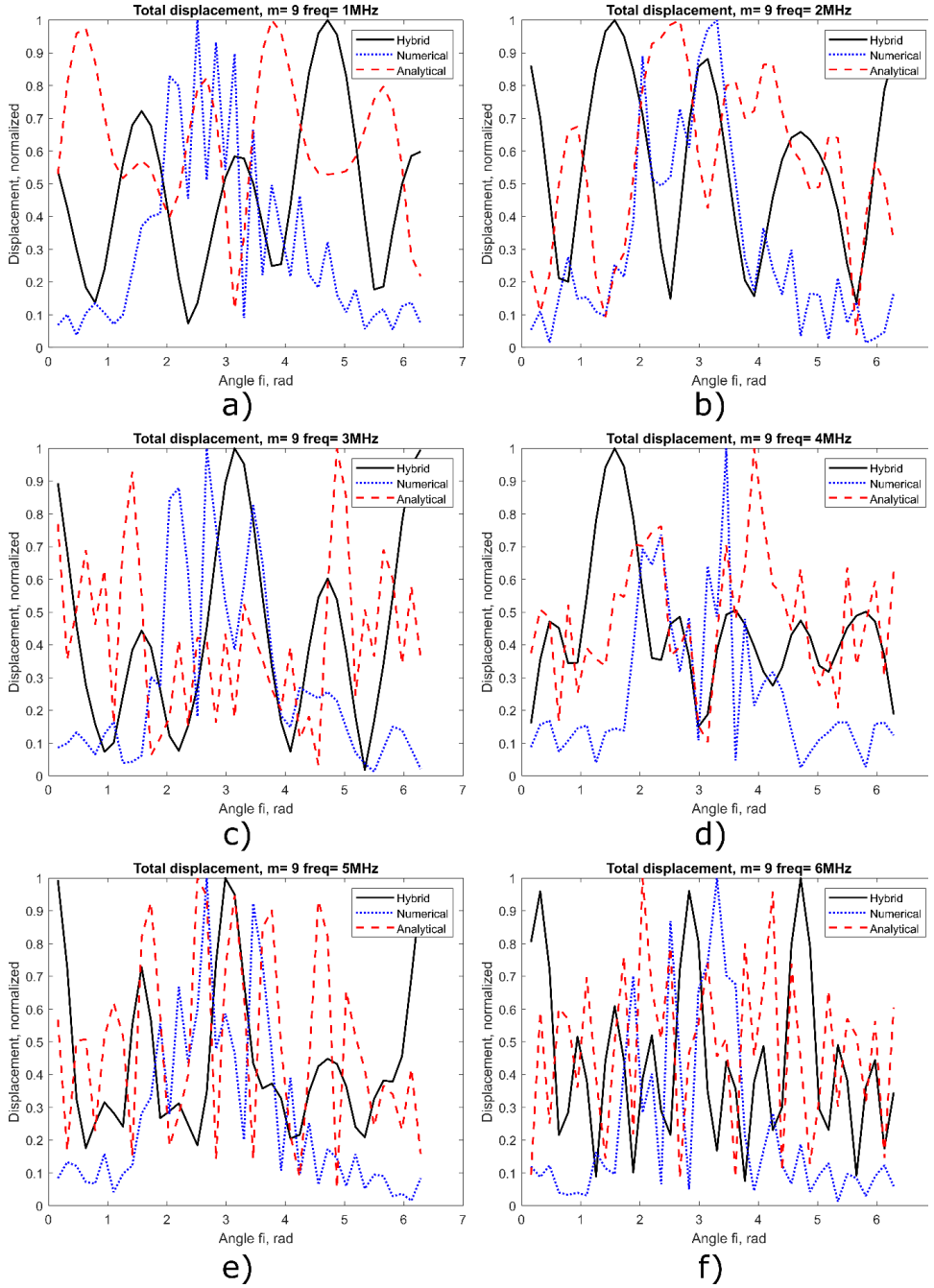


*Fig. 3. Comparison of Hybrid (solid, black), Numerical (dotted, blue) and Analytical (dash, red) solutions for different frequencies with radius of outer circle equal  $2R$*

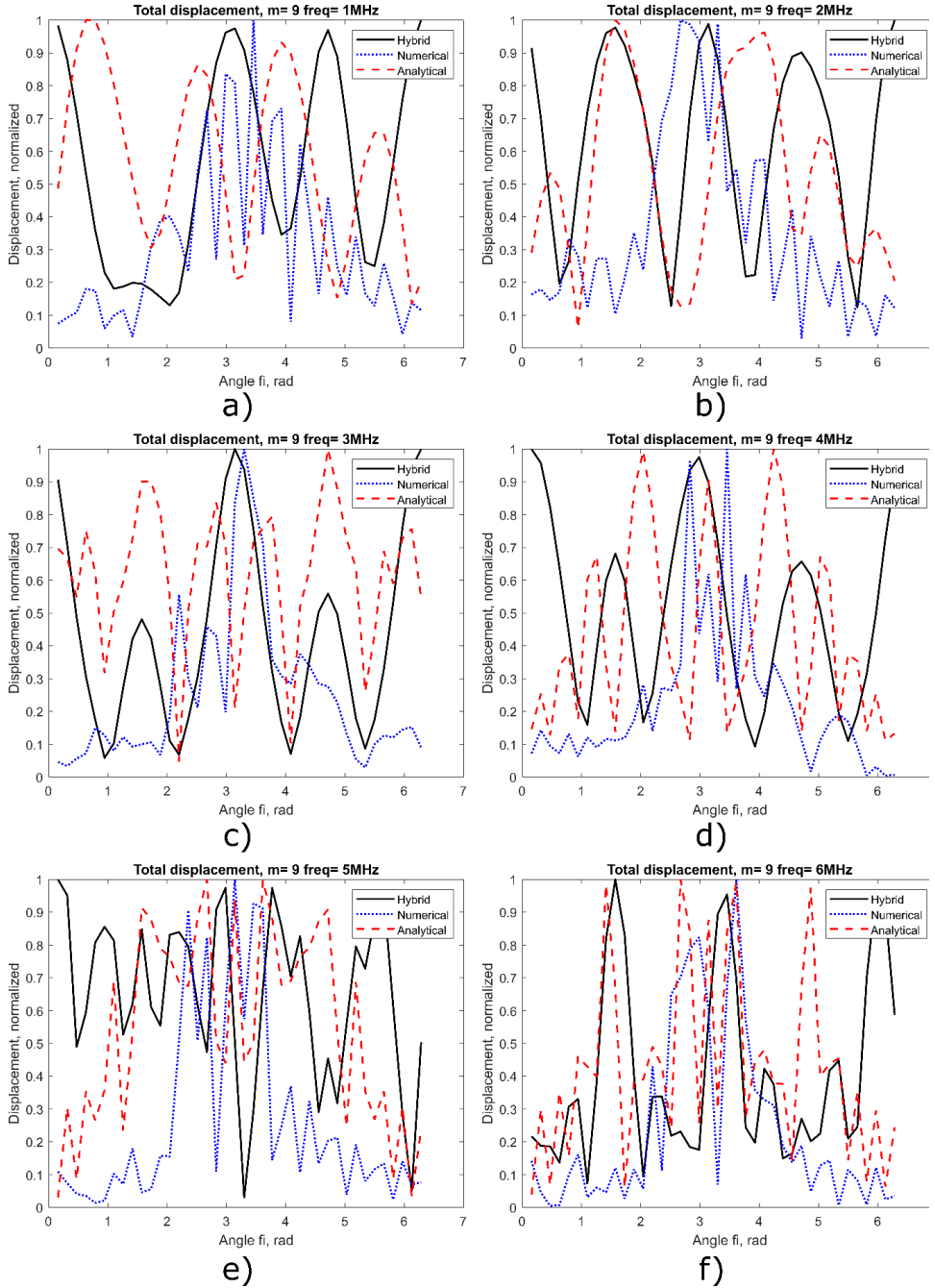


**Fig. 4.** Comparison of Hybrid (solid, black), Numerical (dotted, blue) and Analytical (dash, red) solutions for different frequencies with radius of outer circle equal 1.05R



## 6. Conclusions

In this paper, a newly developed hybrid model is described. This model is based on using semi-analytical and numerical approaches separately for the specific parts of the problem first, and then combining them. The analytical method is used for describing the wave propagation between the probe and the defect, and the numerical solution simulates the interaction between the wave and the complex shape defect by surrounding it with a finite element scheme. The numerical calculations for the 2D hybrid model were done in COMSOL Multiphysics®. The analytical solution, determination of T matrix and further calculations were done in MATLAB®.

The Hybrid model is using T matrix method to combine two approaches. The T matrix contains information about the defect and does not depend on probe configuration or position. Therefore, with T matrix known it is possible to model a scanning inspection situation for the range of frequencies and probe positions. To verify the developed model, comparison with fully numerical and fully analytical results were used. Simulations were done separately for several values of the frequency.

The comparison of the results from Hybrid, Numerical and Analytical solutions is shown to have good agreement in general. The Hybrid solution is located in between the analytical and numerical solutions, as it was expected. This solution has better correlation with numerical part than the analytical one has, especially for the higher frequencies.

The total displacement for hybrid and numerical solution is very similar for the higher frequency values. For the lower frequencies the difference is more obvious, but overall shape of the signal and the positions of the peaks are close enough.

## References

1. R. K. Chapman. A system model for the ultrasonic inspection of smooth planar cracks. *J Nondestruct Eval* 9 (1990), 197-210.
2. P. Fellingner et al. Numerical modeling of elastic wave propagation and scattering with EFIT - elastodynamic finite integration technique. *Wave motion* 21.1 (1995), 47-66.
3. A. Lhémy et al. Modeling Tools for Ultrasonic Inspection of Welds. *NDTE International* 33 (2000), 499 - 513.
4. J. N. Gray et al. *Metals Handbook* 17 (1989), 202.
5. J. D. Achenbach. *Evaluation of Materials and Structures by Quantitative Ultrasonics*. Springer, Wien, 1993.
6. A. Boström and H. Wirdelius. Ultrasonic probe modelling and nondestructive crack detection. *The Journal of the Acoustical Society of America* 97.5 (1995), 2836-2848.
7. P. Bövik and A. Boström. A model of ultrasonic nondestructive testing for internal and subsurface cracks. *The Journal of the Acoustical Society of America* 102.5 (1997), 2723 - 2733.

8. J. Westlund and A. Boström. A Hybrid T Matrix/Boundary Element Method for Elastic Wave Scattering from a Defect Near a Non-planar Surface. *Journal of nondestructive evaluation* 31.2 (2012), 148 - 156.
9. A. Boström, G. Kristensson, and S. Ström. Transformation properties of plane, spherical and cylindrical scalar and vector wave functions. In: V.V. Varadan, A. Lakhtakia, V.K. Varadan (eds) *Field Representations and Introduction to Scattering. Acoustic, Electromagnetic and Elastic Wave Scattering 1* (1991), 165 - 210.
10. J. Westlund and A. Boström. A 2D model of ultrasonic testing for cracks near a non-planar surface. *Wave Motion* 47.6 (2010), 383 - 394.